# GPR143 directs virus-induced cell vacuolation via the MKK6–p38 pathway in teleost

**Qing Wang[13], Jian-Tao Liang[1], Xue-Hong He[1], Li-Yun Wei[1], Xu Yan[1], Yang-Hui Meng[1], Xiu-Ru Zhu[1], Song-Li Qing[1], Hui-Hong Zhao[13], Jin-Hui Wu[2], Qi-Wei Qin[134,*].**

[1] College of Marine Sciences, South China Agricultural University, Guangzhou, Guangdong 511436 , China

[2] Agro-Tech Extension Center of Guangdong Province, Huizhou, Guangdong 511436, China

[3] Fishery Institute of South China Agricultural University, Nansha, Guangzhou 511457, China

[4] Laboratory for Marine Biology and Biotechnology, Pilot National Laboratory for Marine Science and Technology (Qingdao), Qingdao 266000, China

[*] Correspondence: qinqw@scau.edu.cn



Zoological Research

**ABSTRACT**

Causing cytoplasmic vacuolization is a key step for many viruses to induce cell death, however, the underlying mechanisms remain unclear. Nervous necrosis virus (NNV) induces pronounced cytoplasmic vacuoles in the brain during infection. G protein-coupled receptors (GPCRs) regulate autophagosomes and cause vacuolation. Our previous genome-wide association study identified GPR143 as a key candidate gene target for anti-RGNNV approaches in groupers. Here, we used orange-spotted grouper (*Epinephelus coioides*) and red-spotted grouper NNV (RGNNV) as the models to investigate the role of GPR143 in mediating virus induced cellular vacuolation in the central nervous system. The results demonstrate that GPR143 promotes RGNNV-induced cell vacuolation through accelerate binding of autophagosomes and lysosomes. Further investigation revealed that RGNNV facilitates GPR143 binding to MKK6, and MKK6 regulates p38 phosphorylation in the target of rapamycin (m*TOR*) pathway, promoting the binding of autophagosomes and lysosomes to induce cytoplasmic vacuolization. Finally, the zebrafish with GPR143 knockout confirmed that the absence of GPR143 significantly reduces brain vacuolation and fry mortality. These results indicated that GPR143 directs virus-induced cell vacuolation via the MKK6–p38 pathway in teleost. Our study reveals a novel pathway by which viruses cause vacuolation in vertebrates.

**Keywords:** Vacuolation; GPR143 MKK6-p38; RGNNV; Teleost

## INTRODUCTION

Cytoplasmic vacuolation, also termed cytoplasmic vacuolization, is a recognized morphological alteration in cells exposed to viral pathogens as well as various natural and synthetic low-molecular-weight compounds (Aki et al., 2012; Shubin et al., 2016). To date, vacuolation effects from viral infections have been documented across 15 viruses, including hepatitis A virus (HAV), hepatitis C virus (HCV), bovine viral diarrhea virus (BVDV), and encephalomyocarditis virus (EMCV) (Shubin et al., 2016; Chu & Ng, 2003; Krylova & Dzhikidze, 2005; Monel et al., 2007). While current research has largely focused on the mechanisms of cell death and apoptosis associated with cytoplasmic vacuolation, the process underlying the formation of these vacuoles particularly in the context of viral infection remains poorly understood (Aki et al., 2012; Maltese & Overmeyer, 2004; Sharma et al., 2021). Therefore, the mechanisms underlying virus-induced cellular vacuolation require further investigations.

Nervous necrosis virus (NNV), a highly destructive marine virus, typically induces viral nervous necrosis (VNN) or viral encephalopathy and retinopathy (VER) in marine and freshwater fish larvae and juveniles (Soutoet et al., 2019). NNV has recently expanded to over 140 fish species across Europe, Australia, North America, and Asia (Bandín & Souto, 2020; Doan et al., 2017). NNV is classified into four clades: barfin flounder NNV, striped jack NNV, tiger puffer NNV, and red-spotted grouper NNV (RGNNV) (Nishizawa et al., 2020). Among them, RGNNV is the most infectious and destructive (Xu et al., 2010). The typical pathological feature is that the virus-induced vacuolation of cells leads to cell death, which subsequently causes a large amount of vacuolation in the brain and retinal tissues. (Chi et al., 2010). Grouper, being highly susceptible to RGNNV, exhibits severe vacuolation in brain tissues and cells upon infection (Wang et al., 2021a; Wang et al., 2024). Therefore, RGNNV infection in groupers is an ideal model for exploring viruses cause cellular vacuolation in fish.

Our previous genome-wide association study identified GPR143 *as* a key candidate gene target for anti-RGNNV approaches in groupers (Wang et al., 2024). In addition,

the expression level of GPR143 in resistant fish was significantly lower than that of susceptible fish. Moreover, resistant fish showed less severe brain tissue vacuolation compared to susceptible fish (Duan et al., 2014), suggesting a potential role for GPR143 in RGNNV-induced vacuolation. GPR143 associated with ocular albinism type 1 (OA1), belongs to the G protein-coupled receptor (GPCR) family (Schiaffino et al., 1999; Pierce et al., 2002). Growing evidence indicates that GPCRs are exploited by viruses to promote attachment, entry, replication, and egress (Cilliers et al., 2005; Jakobsen et al.,2010; Wang B et al., 2010). Notably, a subset of GPCRs, termed lysosomal GPCR-like proteins—such as LYCHOS (formerly GPR155) and GPR137B—localize to lysosomes and regulate lysosomal function, playing important roles in cellular vacuolation (Gan et al., 2019; Shin et al., 2022). This suggests that lysosomal GPCR-like proteins may be critical in the formation and function of cytoplasmic vacuoles. GPR143 encodes an intracellular GPCR that also localizes to lysosomes (Goshima et al., 2019; Innamorati et al., 2006). Given the involvement of GPCRs in vacuolation and the lysosomal localization of GPR143 we hypothesized that GPR143 plays a key role in RGNNV-induced cytoplasmic vacuolation.

In the present study, we explored the effect of GPR143 on cellular vacuolation induced by RGNNV and revealed the signaling pathway of GPR143 -induced cellular vacuolation in teleosts. The aim of the present study was to explore the role of GPR143 in mediating the molecular mechanisms of cytoplasmic vacuolation during RGNNV infections.

## MATERIALS AND METHODS

### Animals, cell line and viruses

Orange-spotted grouper (*E. coioides*) fry were obtained from Agro-Tech Extension Center of Guangdong Province and cultured for one week before the experiment. Their average weight and length were 2.90±0.32 g and 3.13±0.25 cm, respectively. The grouper were cultured in a 2-t independent tank with circulating water at 25–28◦C, with

a dissolved oxygen (DO) concentration of 5–6 mg O2/L. Fish were fed with grouper fodder twice a day.

A GPR143 mutant zebrafish line was generated using the CRISPR/Cas9-mediated knockout system (Huang et al., 2019). Briefly, the online tool ZiFiT Targeter (v. 4.2; http://zifit.partners.org/ZiFiT/Disclaimer.aspx) was used to design CRISPR/Cas9 target sites. Recombinant plasmids pCS2-nCas9n and DraI-digested pDR274 (Addgene, Cambridge, MA) containing annealed oligonucleotides were used to prepare Cas9 mRNA and single guide RNAs (sgRNAs), respectively. The Ambion mMESSAGE mMACHINE SP6 transcription kit (Invitrogen,USA) was used for *in vitro* transcription. A total of 4.6 nL of a solution containing Cas9 mRNA (300 ng/mL) and sgRNA (50 ng/mL) was co-injected into one- or two-cell stage embryos using a Drummond Nanoject injector (Drummond Scientific, USA). Microinjected embryos were reared at 28°C in freshwater until the adult stage as F0 founders. F0 founders were detected using T7E I (T7 endonuclease I), and mutations were confirmed using sequencing. F1 mutants were inbred to obtain F2 homozygotes. GPR143 expression was assessed using RT-qPCR with mutation-specific primers, and homozygous fish were used for further experiments. Primers are listed in the repository.

The GS cell line, established in our laboratory (Huang et al., 2019), was cultured in Leibovitz's L-15 medium supplemented with 10% fetal bovine serum (FBS; Gibco, USA) at 28°C.

HEK-293T cells were obtained from ATCC, and cultured in Dulbecco’s Modifed Eagle Medium (DMEM, Gibco, USA) supplemented with 10% foetal bovine serum (FBS,Gibco, USA), and maintained at 37◦C with 5% CO2.

All the fish were deeply anesthetized with 100 mg/L MS-222 (Sigma-Aldrich, USA) before dissection. All animal experiments were conducted in accordance with the guidelines and were approved by the appropriate Animal Research and Ethics Committees of South China Agricultural University (SHAUQ202216).

Propagation of RGNNV was performed as described previously (Wang et al., 2021a). For viral stock propagation, GS cells at 80% confluence were inoculated with virus for

2h. After 2h, the cells were washed three times with Leibovitz L15 medium supplemented with 2% FBS to remove excess RGNNV, and Leibovitz L15 medium supplemented with 10% FBS was added. Virus-containing cellular supernatant was harvested 48 to 60 h postinfection, centrifuged to remove cell debris, aliquoted, and stored at -80°C until use. The viral titers of RGNNV were $10^7$ times the 50% tissue culture infective dose ($TCID_{50}$)/ml.

**Plasmid construction**

Total RNA was extracted from the orange-spotted grouper spleen. The total RNA extracted was reverse-transcribed into cDNA using a First Strand cDNA Synthesis Kit (Toyobo, USA). The open reading frames (ORF) cDNA of *gpr143*, *hsc70*, *hsp90ab1*, *lc3*, *lamp1*, and *mkk6* were amplified by PCR using specific primers listed in the repository. The ORF cDNA of GPR143 was subcloned into pEGFP-C1 and pcDNA3.1-3HA vectors. The ORF of HSC70 was subcloned into the pcDNA3.1-3×FLAG vector, and the ORF cDNA of HSP90ab1 was subcloned into a pcDNA3.1-3×FLAG vector. The ORF cDNA of MKK6 was subcloned into pcDNA3.1-3×FLAG, pcDNA3.1-3HA, and pmCherry-C1 vectors. The ORF cDNA of p38α, p38β, p38γ, and p38δ were subcloned into pcDNA3.1-3×FLAG vectors. The ORF cDNA of LC3 was subcloned into pcDNA3.1-3×FLAG and pmCherry-C1 vectors. The ORF cDNA of Lamp1 was subcloned into the pEGFP-C1 vector. Primers used are listed in the repository. Recombinant plasmids were confirmed by DNA sequencing.

**Antibodies**

A rabbit anti-CP antibody prepared in our laboratory was used at a dilution of 1:300 for WB. The specificity of this antibody has been reported previously (Wang et al., 2021). The mouse anti-FLAG antibody (Abmart, China) was used at a dilution of 1:2 000. The mouse anti-HA antibody (Sigma–Aldrich,USA) was used at a dilution of 1:2 000. Anti-MKK6 (Cat# 9264), p38 MAP kinase (Cell Signaling Technology, USA), p-p38MAP kinase (Cat# 8690), anti-phospho-m*TOR* (Ser2448) (Cat# 2971), and anti-m*TOR* (Cat# 2983) were purchased from Cell Signaling Technology and used at a dilution of 1:2 000. Mouse anti-actin antibody (Merck, Germany) was purchased from

Merck and used at a dilution of 1:3 000. The secondary antibodies, goat anti-mouse IgG (Cat# SA00001-1) and goat anti-rabbit IgG (Cat# SA00001-2), were obtained from Proteintech and used at a dilution of 1:3 000.

**_In vivo_ viral infection**

Orange-spotted grouper (*E coioides*) fry were cultured for one week before the experiment. The fish were cultured in a 1-t inde pendent tank with circulating water at 25–28℃, with a dissolved oxygen (DO) concentration of 5–6 mg $O_2$/L. Fish were fed with grouper fodder twice a day. Their average weight and length were 2.90±0.32 g and 3.13±0.25 cm, respectively. Prior to infection, RNA extracted from a mixture of brain, eye, gill, spleen, and head kidney tissues from three randomly selected fish was amplified using specific primers for RGNNV genes to ensure no prior infection. Sixty-five fish were included in the virus infection groups, and 65 fish were used as controls. Fish were injected intraperitoneally with either 20 μL of $10^7$ $TCID_{50}$/ml RGNNV or 20 μL PBS (control group). At 1, 2, and 3 days of inflection with RGNNV, the brains from five RGNNV-infected and PBS-injected fish were collected in buffered 4% paraformaldehyde for histology. Brains from an additional 10 RGNNV-infected and 10 PBS-injected fish were collected for RT-qPCR, and another additional five RGNNV-infected and five PBS-injected fish were collected for WB.

For the p38β inhibition experiment, the following five groups were established: PBS, RGNNV, RGNNV+SB203580, RGNNV+50 μmol/LSB20358 and RGNNV+ 100 μmol/LSB20358. Each group comprised three parallel groups ($n$=20). Fish were injected intraperitoneally with 20 μL of $10^7$ $TCID_{50}$/ml RGNNV 24h after intracranial injection with PBS or different concentrations of SB203580. After 1, 3, and 5 days, 15 fish were randomly selected from each group, and brain tissue was extracted. Brain tissues from five fish were used for western blotting analysis, and tissues from the other five fish were fixed in Bouin's fluid for histological analysis, the remaining five fish were used for RT-qPCR analysis.

For zebrafish challenge experiment, we selected WT and GPR143 zebrafish that had hatched for 5 days for RGNNV immersion challenge. After 24 hours of challenge, the whole fish were collected in liquid nitrogen for rapid freezing and stored at -80℃ for subsequent analysis.

This study had been conducted adhering to the ARRIVE guidelines.

**RNAi performance and SB203580 treatment**

Short interfering RNAs (siRNAs) targeting *gpr143*, *mkk6*, and *mtor* were designed by RiboBio (Guangzhou, China). The siRNA sequences are listed in Table S2. A siRNA with no homology to GPR143 MKK6, or m*TOR* mRNA was used as a control. The knockdown efficacy of the siRNA was analyzed using RT-qPCR (Figure S5). GS cells were seeded into 48-well plates, cultured overnight, and transfected with 0.72 μg/mL GPR143 MKK6, or m*TOR* siRNA or negative control siRNA using Lipofectamine 3 000 (Invitrogen,USA). Cells were infected with RGNNV 24h after transfection and imaged 12h, 24h, and 48h later using light microscopy (Zeiss,Germany) to assess cell morphology, cytopathic effects (CPEs; vacuolation), vacuolar number and the diameter of the vacuoles. After RGNNV infection for 12, 24, and 48h, cells were washed thrice with PBS, and total protein and RNA were extracted for WB and RT-qPCR analyses.

To inhibit p38β, we used the p38 inhibitor SB203580 (Houston, USA). GS cells were seeded into 48-well plates and cultured overnight, treated with 50 μmol/L SB203580 or PBS, infected with RGNNV for 12, 24, and 48h, and then imaged to assess cell morphology, CPEs, vacuolar number and the diameter of the vacuoles using light microscopy (Zeiss,Germany). The cells were washed thrice with PBS, and total protein and RNA were extracted for WB and RT-qPCR analyses.

**Fluorescence microscopy**

To investigate the cellular localization of GPR143 and CP, GS cells were co-transfected with *GFP-GPR143* and *Cherry-CP* plasmids using Lipofectamine 3 000 reagent for 24h. The cells were stimulated with RGNNV for 24h, washed twice with Hank's balanced salt solution, and fixed in 4% paraformaldehyde in PBS for 15 min at room temperature. The cells were then washed thrice with PBS, treated with DAPI to stain the nuclei, and observed under an inverted fluorescence microscope

(Zeiss,Germany).

To examine the binding time of GPR143 to LC3 or Lamp1 induced by RGNNV, GS cells were co-transfected with *GFP-GPR143* and *Cherry-LC3*-or *GFP-GPR143* and Cherry -Lamp1 plasmids using Lipofectamine 3 000 reagent for 24h. The cells were stimulated with RGNNV for 1,3, 6, 9, 12 and 24h, washed twice with Hank's balanced salt solution, and fixed in 4% paraformaldehyde in PBS for 15 min at room temperature. The cells were then washed thrice with PBS, treated with DAPI to stain the nuclei, and observed under an inverted fluorescence microscope (Zeiss,Germany).

To investigate the binding of LC3 to Lamp1 under different treatment conditions, GS cells were co-transfected with *GFP-LC3* and *Cherry-Lamp1* or *GFP-LC3*, Cherry-Lamp1, and GPR143 siRNA, or *GFP-LC3*, Cherry- Lamp1, and MKK6 siRNA, or *GFP-LC3*, Cherry- Lamp1, and m*TOR* siRNA using Lipofectamine 3 000 reagent. Cells were also co-transfected with *GFP-LC3* and *Cherry-Lamp1* and stimulated with SB203580. The cells were stimulated with RGNNV for 24h, washed twice with Hank's balanced salt solution, and fixed in 4% paraformaldehyde in PBS for 15 min at room temperature. The cells were then washed thrice with PBS, treated with DAPI to stain the nuclei, and observed under an inverted fluorescence microscope (Zeiss,Germany).

To determine the subcellular localization of *GPR143 LC3*, *Lamp1*, *CP*, and *MKK6*, the ORF cDNA of these genes was cloned into the corresponding plasmids. The plasmid construction was previously described. Plasmids were transfected or co-transfected into GS cells. After 48h of culture, cells were fixed with 4% paraformaldehyde and stained with 6-diamidino-2-phenylindole (DAPI) (1 mg/ml) for 15 min. Cells were then rinsed with PBS, mounted with 50% glycerol, and observed using fluorescence microscopy (Leica, Germany).

**Immunofluorescence assay**

HEK293T or GS cells were seeded in glass-bottomed cell culture dishes and transfected with the recombinant plasmid. At the indicated time points, cells were

infected with RGNNV, fixed in 4% paraformaldehyde for 1h, and permeabilized with 0.2% Triton X-100 for 15 min. After washing thrice with PBS, the cells were blocked with 2% bovine serum albumin (BSA) for 45 min and then incubated with anti-CP serum (prepared in our laboratory 1:200) for 2h at room temperature. The cells were washed with PBS and incubated with a secondary antibody (fluorescent isothiocyanate-conjugated goat anti-rabbit immunoglobulin G, Pierce) for 1h at room temperature. Cells were then stained with DAPI and observed under an inverted fluorescence microscope (Zeiss,Germany).

**Fluorescence *in situ* hybridization (FISH)**

Fluorescence *in situ* hybridization (FISH) was performed following previously described protocols (Lai et al., 2020; Lauter et al., 2011). Probes were synthesized from the ORF sequences of *gpr143*, *mkk6*, and *p38β* using an RNA labeling kit (Roche Diagnostics). Primer sequences are listed in the repository. Briefly, brain tissues from grouper or zebrafish were fixed in buffered 4% paraformaldehyde overnight at 4°C, rinsed twice with cold PBS, transferred to a 30% sucrose solution for 48h, and stored at 4°C. Samples were dried with sucrose, frozen on dry ice, and embedded in an OCT compound (Sakura, USA). Tissue sections were prepared at −21°C, attached to cationic anti-off slides (Thermo Fisher Scientific), covered, and incubated at 42°C for one day. Sections were prehybridized for 30 min, followed by the addition of 250 μL hybridization buffer containing 150 ng of DIG-labeled sense or antisense GPR143 MKK6, and P38β riboprobe to each slide. Slides were incubated in a humidified box at 42°C for 16h. Post-hybridization, sections were sequentially washed twice in 2× saline-sodium citrate (SSC) (1×SSC=0.15 M NaCl, 15 mM Na citrate) at room temperature for 15 min, in 1×SSC and 0.1×SSC at 55°C for 1h. Slides were then mounted using Fluoroshield with DAPI (Sigma–Aldrich). Fluorescent signals were imaged using a Zeiss confocal microscope (Oberkochen, Germany).

**Immunoprecipitation-mass spectrometry**

GS cells were transfected with pcDNA3.1-3×HA or *GPR143* -3×HA for 24h, followed by RGNNV infection for 48h. Cells were collected and stored at −80 ℃. Mass spectrometry was performed using a Q Exactive Plus mass spectrometer (Thermo Scientific) coupled with an EASY-nLC 1 200 liquid chromatography system (Thermo Scientific). Mass spectral data were analyzed using MaxQuant (v.1.6.6) software.

**Co-immunoprecipitation assays**

Protein interactions were verified by co-transfecting GPR143 -3×HA or MKK6-3×HA with CP-3×FLAG, MKK6-3×FLAG, p38α-3×FLAG, p38β-3×FLAG, p38γ-3×FLAG, or p38δ-3×FLAG plasmids. After 36h, cells were lysed in immunoprecipitation (IP) lysis buffer with a protease inhibitor cocktail. Lysates were centrifuged at 12 000 × g for 5 min, and supernatants were collected for western blotting and immunoprecipitation using a Dynabeads™ protein G immunoprecipitation kit (Invitrogen,USA). Briefly, magnetic beads were prepared and bound to anti-HA or anti-FLAG antibodies for 10 min at room temperature, then incubated with antigen-containing samples for 30 min. After washing, target antigens were eluted and subjected to western blotting. Primary antibodies specific to FLAG or HA were used to detect protein expression and interactions.

**Western blotting**

Cells or brain tissues were washed with PBS and resuspended in IP lysis buffer (Invitrogen,USA). Whole-cell lysates were separated by sodium dodecyl sulfate-polyacrylamide gel electrophoresis and transferred onto polyvinylidene fluoride membranes (Millipore). Membranes were blocked for 1h at room temperature in 5% skim milk or 3% BSA dissolved in PBS, then incubated with primary antibodies for 2h at room temperature. After washing with PBS containing 0.1% Tween 20 (PBST), membranes were incubated with horseradish peroxidase-coupled secondary antibodies

(KPL). After washing with PBST thrice, antigens were detected using an enhanced chemiluminescence (ECL) detection reagent (Thermo Fisher Scientific).

**RNA extraction and real-time quantitative polymerase chain reaction (RT-qPCR)**

Cells or brain tissues were collected, and total RNA was extracted using 500 μl TRIzol (Invitrogen,USA) and 200 μl chloroform. The total RNA from brain tissue was extracted by adding 1 000 μl of TRIzol and 200 μL of chloroform. After centrifugation at 12 000 rpm for 15 min at 4°C, the supernatant was transferred to an RNase-free 1.5-mL tube. Isopropanol and 75% alcohol were used for RNA precipitation and purification. Total RNA was reverse-transcribed to synthesize first-strand cDNA using the ReverTra Ace kit (TOYOBO, Japan) following the manufacturer's instructions. RT-qPCR amplification was performed on an ABI QuantStudio 5 system (Applied Biosystems, USA) using SYBR green real-time PCR mix (TOYOBO). β-actin was used as the internal control to verify successful transcription and calibrate the cDNA template for the corresponding samples. Each assay was performed in triplicate with the following cycling conditions: 1 min for activation at 95°C followed by 40 cycles of 15 s at 95°C, 15 s at 60°C, and 45 s at 72°C. Triplicate CT values were calculated using the comparative CT ($2^{-\Delta\Delta Ct}$) method (Livak & Schmittgen, 2001). Data are presented as the mean ±standard deviation (SD). All reagents were pre-cooled. RT-qPCR results were calculated based on the expression levels of target genes normalized to that of β-actin at the indicated times. Primers used for qPCR are listed in the repository.

**Virus titers**

Virus titers. The titers of the RGNNV viral stocks were determined by the $TCID_{50}$ as described previously (Wang Q et al., 2021). In short, GS cells were seeded in 96-well plates 1 to 2 days prior to inoculation to allow a full monolayer to form. RGNNV viral stocks were thawed on ice, viral stocks were diluted via 10-fold dilutions, and inoculation was performed. After 2h, the inoculation medium was washed off and

replaced with Leibovitz L15 medium supplemented with 10% FBS. Plaques were counted 1 day postinfection, and titers were calculated using the Reed-Muench method.

**Brain histology**

Brains were dissected from susceptible and resistant groupers, PBS-, RGNNV-, and RGNNV+SB203580-treated groupers, and PBS- or RGNNV-treated WT and GPR143 zebrafish. The brains were fixed in Bouin's solution for 24h at room temperature, dehydrated, and embedded in paraffin wax. All tissue blocks were sectioned at 5 μm and stained with hematoxylin and eosin for analysis.

**Survival assay**

Three parallel groups of fish treated with PBS, RGNNV, or RGNNV+50μmol/L SB203580 ($n$=50 fish/group), were injected intraperitoneally with 20 μL of $10^7$ $TCID_{50}$/ml RGNNV 24h after intracranial injection with PBS or SB203580. Deaths were recorded daily for 14 days. Parallel groups of 5-day post-fertilization WT and GPR143 zebrafish were treated with PBS or RGNNV. Deaths were recorded daily for 14 days.

**Statistical analysis**

The results are presented as the mean ± SD. Statistical comparisons were performed using a Student's t-test, one-way analysis of variance (ANOVA), or two-way ANOVA. $P$-values of <0.05, <0.01, and <0.000 1 were considered statistically significant and highly statistically significant, respectively.

# RESULTS

**GPR143 promotes RGNNV-induced cell vacuolation**

We investigated the role of GPR143 in RGNNV-induced vacuolization by comparing brain tissues from RGNNV-infected and PBS-injected groupers. Vacuoles were evident

355 in the brain tissue of infected fish (Fig. 1A), and their number increased over 1–3 days
356 post-infection (Figure 1B). Additionally, expression of the viral capsid protein (CP) in
357 brain tissue rose with prolonged infection time (Figure 1C). *gpr143* expression was also
358 significantly upregulated ($P < 0.000\ 1$) in RGNNV-infected fish compared with
359 uninfected controls (Figure 1D). Using an RGNNV-susceptible GS cell line, we found
360 that GPR143 overexpression enhanced vacuolization relative to RGNNV infection
361 alone, whereas GPR143 knockdown via siRNA reduced vacuole formation (Figure 1E).
362 Conversely, inhibiting GPR143 expression with siRNA resulted in fewer vacuoles than
363 that in the RGNNV-only group (Figure 1E). However, based on WB and RT-qPCR
364 detections of CPs and virus gene expression, the overexpression or inhibition of
365 GPR143 had no significant effect on the replication of RGNNV (Figure 1, F-H).
366 Consistently, viral titers were not markedly altered by GPR143 modulation (Figure 1 I).
367 Together, these results demonstrate that GPR143 promotes RGNNV-induced
368 vacuolization without substantially influencing viral replication.
369
370 **GPR143 binds to RGNNV CP but is not a receptor**
371 We explored the involvement of GPR143 in RGNNV-induced brain tissue
372 vacuolation by investigating its binding to RGNNV CPs. *In situ* hybridization showed
373 co-expression of *gpr143* and *cp* genes in RGNNV-infected fish brain cells, with no co-
374 expression of *gpr143* and *cp* in the brain of PBS-injected fish (Figure 2A). Co-
375 immunoprecipitation assays confirmed that GPR143 co-precipitated with CP (Figure 2,
376 B, C). Considering GPR143 is a transmembrane protein, we hypothesized that it could
377 be an RGNNV receptor. To validate this hypothesis, we transfected HEK293T cells
378 with FLAG-tagged GPR143 alone or in combination with known RGNNV receptors
379 HSC70 or HSP90ab1, and then assessed viral gene expression after RGNNV challenge.
380 Transfection of GPR143 alone did not enhance viral gene expression, but co-
381 transfection with GPR143 and either HSC70 or HSP90ab1 significantly increased it
382 (Figure 2D; Figure S1, A–D). Immunofluorescence results were consistent, showing no

CP-positive signal with GPR143 alone but a positive signal with co-transfection (Figure S1 E). Similar experiments in GS cells showed that viral gene expression in the GPR143 -alone group was comparable with that in the control but significantly increased with co-transfection (Figure 2D ; Figure S2, A–D). Immunofluorescence confirmed the findings above (Figure S2 E). In addition, co-transfection of *GFP-GPR143* and *Cherry-CP* plasmids in GS cells revealed co-localization of GPR143 and CP after RGNNV stimulation, also indicating that GPR143 binding occurs within the cell rather than on the surface (Figure 2E). These results demonstrate that GPR143 binds to CP but is not a receptor for RGNNV.

**GPR143 plays a critical role in the binding of autophagosomes and lysosomes**

We investigated the role of GPR143 in RGNNV infection by examining its localization in both infected and uninfected brain tissues. Following viral infection, GPR143 was found to accumulate around vacuolar structures (Figure 3A), indicating its involvement in virus-induced vacuolation. We further examined whether GPR143 contributes to vacuolation in previously identified RGNNV target cells, GLU1 and GLU3 (Wang et al., 2021b). The results showed that RGNNV infection induced aggregation of GPR143 in target cells at 12 and 24hours post-infection (hpi), followed by the onset of vacuolation at 48 hpi. (Figure 3B). To elucidate the role of GPR143 in vacuole formation, we analyzed its localization relative to the autophagosome marker LC3 and the lysosome marker LAMP1. In uninfected cells, GPR143 co-localized with autophagosomes, which enlarged after viral infection (Figure 3C). However, GPR143 did not co-localize with lysosomes until post-viral infection (Figure 3C). Further analysis revealed limited autophagosome-lysosome binding in uninfected cells, which increased over time after RGNNV infection (Figure 3D). Conversely, siRNA knockdown of GPR143 in GS cells led to a significant decrease in autophagosome and lysosome binding post-viral infection (Figure 3E), suggesting that GPR143 is crucial for this process. Additionally, GPR143 bound to LC3 1h post-infection but did not bind

to LAMP1 until 12h post-infection (Figure S3), indicating that GPR143 binds to autophagosomes earlier than lysosomes. The binding of autophagosomes and lysosomes occurred 12h post-RGNNV infection (Figure S3), suggesting that GPR143 initially binds to the autophagosome and subsequently to the lysosome through autophagosome-lysosome binding.

**GPR143 regulates RGNNV-induced vacuolization via MKK6**

To explore the mechanisms by which GPR143 promotes vacuolization during RGNNV infection, changes in GPR143 -binding proteins under RGNNV infection were detected under immunoprecipitation-mass spectrometry (IP-MS) in GS cells. Three proteins exhibited enhanced binding to GPR143 in infected cells compared with uninfected controls (Table S1). Among the corresponding genes *AOC2*, *THRA*, and *MKK6*, only *MKK6* showed significantly elevated expression in the brains of RGNNV-infected fish relative to uninfected controls (Figure 4A; Figure S 4, A, B). Overexpression of GPR143 in GS cells also led to a significant increase in *mkk6* expression (Figure 4B; Figure S4, C, D). Consistent with these findings, Western blot analysis revealed higher MKK6 protein levels in RGNNV-infected brain tissue compared with controls (Figure 4C), and GPR143 overexpression similarly upregulated MKK6 protein in GS cells (Figure 4D). Two-color *in situ* hybridization showed co-localization of *gpr143* and *mkk6* in the brain post-RGNNV infection (Figure 4E). Co-transfection of GFP-GPR143 and Cherry-MKK6 plasmids into GS cells confirmed co-localization post-RGNNV stimulation (Figure S4 E). Co-immunoprecipitation further demonstrated the binding of GPR143 to MKK6 (Figure 4F, G). Two-color *in situ* hybridization indicated co-localization of *gpr143* and *mkk6* around vacuolar structures in RGNNV-infected grouper brain tissue (Figure 4H). These results suggest that GPR143 regulates vacuolization through MKK6 post-RGNNV infection.

**MKK6 regulates RGNNV-induced cellular vacuolation via p38**

MKK6 reportedly significantly regulates p38 (Jin et al., 2006; Wang et al., 2021c). In groupers, four p38 isoforms exist: α, β, γ, and δ (Cai et al., 2011; Sun et al., 2017). Using RT‑qPCR, we measured the mRNA expression of these isoforms in brain tissue following RGNNV challenge. The results demonstrated a significant increase in the expression levels of *p38α*, *p38β*, and *p38γ*, particularly *p38β* (Figure 5A), whereas that of *p38δ* also increased but not significantly. We detected the binding of MKK6 to P38α, P38β, and P38γ via Co-IP (Figure 5 B-E), with binding increasing post-RGNNV infection. These findings suggest that the MKK6–P38 pathway is crucial for RGNNV-induced cellular vacuolation.

To further assess the contribution of P38 to this process, we examined the phosphorylation status of P38β, the most strongly induced isoform. Phosphorylation of p38β increased following RGNNV infection (Figure 5F). We then injected groupers with different concentrations of the p38β inhibitor SB203580 (10 μmol/L, 50 μmol/L, and 100 μmol/L) and challenged them with RGNNV for 1, 3, and 5 days. Treatment with 50 μmol/L and 100 μmol/L SB203580 significantly reduced vacuolation in brain tissue (Figure 5, G, H). However, the SB203580 treatment had no significant effect on virus replication, only reducing virus replication at 100 μmol/L (Figure 5, I, J). These results support a critical role for p38β in RGNNV-induced brain vacuolation. We further investigated the relationship between GPR143 MKK6, and p38β using *in situ* hybridization, revealing co-localization and clustering around vacuoles post-RGNNV infection, with the p38β inhibitor reducing such aggregation (Figure 5K). In addition, the 50 μmol/L SB203580 treatment reduced fry mortality (Figure 5L). siRNA knockdown of *gpr143* or *mkk6* in GS cells inhibited RGNNV-induced p38β phosphorylation (Figure 6, A, B). Interestingly, inhibition of p38β with SB203580 did not disrupt the interaction between GPR143 and MKK6 (Figure 6C), but it significantly reduced autophagosome-lysosome binding (Figure 6D), and decreased the number of RGNNV-induced vacuoles at 12, 24, and 48 hours post-infection (Figure 6, E, F, H).

However, the SB203580 treatment had no significant effect on vacuoles size and virus replication *in vitro* (Figure 6, G, I- L). These results suggest that the GPR143 –MKK6 pathway regulates RGNNV-induced vacuolization via p38.

**The GPR143–MKK6–p38 pathway requires mTORC1 participation for RGNNV-induced vacuolization**

P38 regulates m*TOR*C1 function in mammals, which is vital in lysosomal activation and migration. We investigated P38-mediated regulation of m*TOR*C in RGNNV-induced vacuolation and observed increased m*TOR*C phosphorylation in grouper brain tissue post-RGNNV infection (Figure 7A). Inhibiting *gpr143* and *mkk6* expression by siRNA or P38β activity by SB203580 showed inhibited m*TOR*C phosphorylation (Figure 7B). In GS cells, inhibiting *gpr143*, *mkk6*, or *mtorc* reduced lysosome-autophagosome fusion (Figure 7C) and RGNNV-induced vacuolation number (Figure 7D, E, G), but have no effect on vacuoles size (Figure 7 H), indicating GPR143 and MKK6 as upstream regulators of mTORC. We also detected the effects of siGPR143 siMKK6, and simTORC on virus replication, and the results showed that silencing these genes does not have a considerable effect on viral replication, excluding simTORC, which reduces viral replication (Figure 7, F, I-K).

**Mutational analysis in zebrafish confirms the role of GPR143 in RGNNV-induced vacuolization**

To assess the role of GPR143 in RGNNV-induced vacuolization in vivo, we generated GPR143 mutant zebrafish using a CRISPR/Cas9-mediated knockout system. The zebrafish GPR143 gene consists of eight exons and seven introns (Figure 8 A). We targeted the helix–loop–helix domain encoded by exon 1 and established a stable frameshift mutant line carrying a 4-bp substitution and a 9-bp deletion for subsequent phenotypic analysis (Figure 8B, Figure S6). RT‑qPCR with mutant-specific primers confirmed amplification in wild-type (WT) and heterozygous fish, but not in

homozygous mutants (Figure 8 B, Figure S6). RT-qPCR using mutant-specific primers showed a signal in wild-type (WT) and heterozygous fish, but not in mutants (Figure 8 C).

We next measured the expression of *mkk6* and *p38β* in the brains of WT and GPR143$^{-/-}$ zebrafish after RGNNV challenge. In WT fish, RGNNV infection significantly increased the expression of both *mkk6* ($P$=0.000 8) and *p38β* ($P$=0.0013). By contrast, in GPR143$^{-/-}$ fish, their expression remained unchanged upon infection (Figure 8, D, E). Using in situ hybridization, we also examined the interaction between *mkk6* and *p38β* in brain tissues. RGNNV infection induced clear co-localization of MKK6 and p38β in WT zebrafish, but this effect was absent in GPR143mutants (Figure 8 F).

Further, histological sections and apoptosis assays indicated that RGNNV infection in WT zebrafish resulted in brain tissue vacuolation and resulted in a large number of apoptotic signals (Figure 8, G, H). However, in GPR143$^{-/-}$ zebrafish, RGNNV infection resulted in minimal vacuolation, although apoptotic signals were detected (Figure 8, G , H), suggesting that GPR143 knockout reduces RGNNV-induced brain tissue vacuolation.

Finally, we performed a 5-day immersion challenge with RGNNV in post-hatched WT and GPR143$^{-/-}$ zebrafish. Mortality reached approximately 30% in WT fish, compared to only about 12% in GPR143 mutants (Figure 8 I). Viral replication was not significantly affected by GPR143 knockout (Figure 8, J, K). These results suggest that GPR143 is a critical component in RGNNV-induced brain vacuolation and injury.

## Discussion

RGNNV is known to trigger vacuolation and necrosis in the central nervous system of larval and juvenile marine finfish worldwide (Doan et al., 2011; Ransangan & Manin, 2010; Yong et al., 2017). RGNNV primarily infects the central nervous system of fish, causing significant brain tissue damage, leading to extensive vacuolation within 4–6 days post-infection. In contrast, other viruses that infect the vertebrate nervous

system—such as Reptarenavirus in reptiles and avian influenza virus in birds—do not cause comparably rapid or severe brain pathology (Koyuncu et al., 2013). Some viruses exhibit incubation periods exceeding 10 years and rarely inflict severe brain tissue damage over a short duration, suggesting a unique mechanism by which RGNNV induces extensive brain vacuolation. A previous study used LC3 to label autophagosomes and LAMP1 to label lysosomes reported that CP would impair the binding of autophagosomes and lysosomes through the HSP90ab1-AKT-M*TOR* pathway, thereby inducing incomplete autophagy (Zhang et al., 2022b). Autophagy is the key factor that induces cellular vacuolation; however, the precise mechanism underlying RGNNV-induced cellular vacuolation remains elusive.

We previously conducted a genome-wide association study and identified GPR143 as a critical protein in RGNNV-resistant groupers (Duan et al., 2024). GPR143 is widely expressed in the retina and central nervous system (Goshima et al., 2019; Masukawa et al., 2014) and appears to play a major role in RGNNV infection and vacuolation. We found that GPR143 binds more extensively to CP in the brain tissue of RGNNV-infected fish. While multiple studies have characterized GPR143 as an intracellular GPCR (Schiaffino et al., 1999; Samaraweera et al; 2001; Innamorati et al., 2001), recent studies have shown that GPR143 is localized within melanosomes and lysosomes (Innamorati et al., 2001; Goshima et al., 2019). This suggests that GPR143 is not a protein located on the outer membrane. Our research has found that overexpression of GPR143 in 293T cells which bound RGNNV receptor cannot increase the number of viruses entering the cells. In addition, overexpression of GPR143 in grouper spleen cell lines did not increase the entry of RGNNV into the cells. These indicate GPR143 is not a receptor. However, GPR143 accumulates around vacuoles in RGNNV-infected brain tissue, and inhibition of GPR143 reduces RGNNV-induced vacuolation, whereas increased GPR143 expression exacerbates vacuolation. These results highlight the pivotal role of GPR143 in RGNNV-induced vacuolation.

Virus-induced vacuolation of cells is primarily related to autophagy. Various viruses

employ diverse strategies to regulate autophagy. Viral CPs often initiate autophagic responses by binding to membrane proteins, such as NECTIN4 in peste des petits ruminants virus and heat shock protein 90AA1 in influenza A virus (Yang et al., 2020; Wang et al., 2020b). Some viruses encode proteins that modulate autophagy, such as Nef in HIV and ICP34.5 in herpes simplex virus 1(Kyei et al., 2009; Orvedahl et al., 2007). Our findings suggest that RGNNV initially binds to GPR143 to regulate cellular vacuolation. While GPCRs often function as viral receptors on cell membranes, facilitating attachment, entry, replication, and egress (Cilliers et al., 2005; Jakobsen et al., 2010; Wang et al., 2020a), GPR143 is predominantly localized in intracellular membranes in mammals (Innamorati et al., 2006; Samaraweera et al., 2001). Viruses can bind to intracellular membrane proteins in lysosomes or autophagosomes (Ueo et al., 2020; Zhou et al., 2011), and GPCRs on these organelles play crucial roles in their function and interactions (Gan et al., 2019; Shin et al., 2022; Zhang et al., 2022a).

Autophagy, a critical cellular catabolic process, maintains cellular homeostasis by degrading long-lived proteins and damaged organelles within lysosomes (Boya & Reggiori, 2013; Maiuri et al., 2007; Mizushima et al., 2007). Autophagy begins with the formation of autophagosomes, which eventually fuse with lysosomes to form autolysosomes (Boya & Reggiori, 2013; Yu et al., 2018). Our findings revealed that GPR143 binds to RGNNV CP on intracellular membranes. In GS cells, GPR143 co-localizes with LC3 (expressed in autophagosomes and autolysosomes) but not with LAMP1 (expressed in lysosomes and autolysosomes) in the absence of RGNNV infection. Post-infection, GPR143 co-localizes with LAMP1, and LC3 binds to LAMP1; however, inhibiting GPR143 prevents LC3 from binding to LAMP1. This indicates that RGNNV CPs bind to GPR143 intracellularly, and GPR143 is crucial for regulating autophagosome-lysosome fusion post-RGNNV infection.

Autophagy regulation involves various signaling pathways, including the serine/threonine kinase m*TOR*, which is integral to autophagy in mammalian cells (Li Y et al., 2015). The m*TOR* pathway is closely associated with virus-induced autophagy

578 and interacts with upstream signals, such as PI3K/AKT, AMPK, and MAPK, to initiate
579 autophagy. MAPK pathways are key regulators of autophagosome formation in
580 eukaryotic cells (Madeo et al., 2015).

581 MKK6 receives upstream signals that regulate downstream activation of MAPK in
582 the cytoplasm and nucleus (Li et al., 2016; Raingeaud et al., 1996). In mammalian
583 species, various proteins bind to MKK6 to activate downstream pathways, such as the
584 tumor suppressor protein, LRRK2, and Jhdm1b (Hsu et al., 2010; Wang et al., 2019).
585 Our results showed that MKK6 combines with GPR143 and that GPR143 and MKK6
586 co-localize around brain vacuoles after RGNNV infection, indicating that GPR143
587 regulates RGNNV-induced vacuolization through MKK6.

588 MKK6 is a central regulatory protein responding to environmental and physiological
589 stimuli (Chabaud-Riou & Firestein, 2004; Chang & Karin, 2001). MKK6 is reportedly
590 activated in mice and *Litopenaeus vannamei* in response to environmental stress,
591 bacteria, and viruses (Li et al., 2016; Hammaker et al., 2012; Huang et al., 2011;
592 Yoshizawa et al., 2009; Raingeaud et al., 1995). Mammalian MKK6 activates p38 in
593 response to environmental stress and inflammation and specifically activates p38
594 MAPK isoforms (Raingeaud et al., 1995; Enslen et al., 1998; Yan et al., 2024). In
595 groupers, four p38 isoforms exist: α, β, γ, and δ (Wang et al., 2021c; Cai et al., 2011).
596 Bacterial and viral infections activate p38 (Shi et al., 2014; Yan et al., 2013). In the
597 MAPK signaling pathway, MKK6 receives upstream signals that phosphorylate
598 threonine and tyrosine residues in TGY motifs of downstream p38 MAPKs, activating
599 downstream transcription factors and specific target gene expression (Dashti et al., 2001;
600 Kim et al., 2010; Qu et al., 2019). Our study suggests that MKK6 plays a vital role in
601 RGNNV-induced cellular vacuolation; however, the specific p38 isoform(s) involved
602 remain unknown. In this study, we observed that after RGNNV infection, MKK6
603 induces p38β phosphorylation, and inhibition of p38β reduces RGNNV-induced
604 vacuolation. These results indicate that RGNNV-induced cellular vacuolation is mainly
605 regulated by the GPR143 –MKK6–p38β pathway.

Cellular vacuolation is often caused by autophagy, which begins with the formation of phagophores that form double-membrane-delimited autophagosomes by elongating and enclosing cytoplasmic constituents. The binding of lysosomes to autophagosomes is crucial in autophagy. In mammals, mTORC regulates lysosomal migration and activity. GPCRs primarily regulate the function of mTORC in lysosomal migration (Gan et al., 2019; Shin et al., 2022). p38 plays a crucial role in regulating mTORC (Romero-Becerra et al., 2022; Wang et al., 2022). Our findings revealed that RGNNV infection increases mTORC phosphorylation, and inhibition of GPR143 MKK6, or p38β significantly inhibits RGNNV-induced mTORC phosphorylation, thus inhibiting lysosome-autophagosome binding. This suggests that RGNNV may regulate lysosome and autophagosome binding by modulating mTOR phosphorylation through the GPR143 –MKK6–p38β pathway.

In conclusion, the present study has elucidated a novel mechanism by which RGNNV induces cytoplasmic vacuolation in teleosts through the GPR143 -MKK6-P38–mTOR pathway. Initially, RGNNV enters the cell through acceptor; the RGNNV CP then binds to GPR143 Subsequently, CP binds to GPR143 to facilitate GPR143 binding to MKK6 and promotes p38 phosphorylation. Afterward, p38 phosphorylation targets the mTOR pathway to promote autophagosome-lysosome binding, thereby inducing cytoplasmic vacuolation (Figure 9). Collectively, our findings revealed that RGNNV induces cytoplasmic vacuolation in fish. Our findings may offer a novel therapeutic approach for mitigating the effects of RGNNV and other similar viral infections on marine fish.

## SUPPLEMENTARY DATA

Supplementary data to this article can be found online.

## COMPETING INTERESTS

The authors declare that they have no competing interests

## ACKNOWLEDGMENTS

This work was supported by Guangdong S&T Program (2025B0202080001), the National Natural Science Foundation of China (42176103, U20A20102), the Guangdong Provincial Natural Science Foundation (2022A1515012505), Research on Breeding Technology of Candidate Species for Guangdong Modern Marine Ranching (2024-MRB-00-001), the National Key Research and Development Program of China (2022YFD2400502), and Zhuhai Social Development Science and Technology Project (2420004000111).

## AUTHORS' CONTRIBUTIONS

Q.W., and Q.W.Q. Conceptualization. X.H.H., and J.H.W. Data curation. Q.W., L.Y.W., and Y.H.M. Formal analysis. Q.W., and Q.W.Q. Funding acquisition. H.H.Z. Investigation. Q.W. Writing – review & editing. J.T.L., X.H., X.Y., X.R.Z., and J.H.W. Methodology. J.T.L: Writing – original draft. X.Y. Software. Q.W.Q. Validation. Q.W. Q. Project administration. All authors read and approved the final version of the manuscript.

## References


Aki T, Nara A, Uemura K. 2012. Cytoplasmic vacuolization during exposure to drugs and other substances. *Cell Biol Toxicol*. 28:125–131.

Bandín I, Souto S. 2020. *Betanodavirus* and VER disease: A 30-year research review. *Pathogens*. 9:106.

Boya P, Reggiori F, 2013. Codogno P. Emerging regulation and functions of autophagy. *Nat Cell Biol*. 15:713–720.

Cai J, Huang Y, Wei S, et al. 2011. Characterization of p38 MAPKs from orange-spotted grouper, *Epinephelus coioides* involved in SGIV infection. *Fish Shellfish Immunol*. 31:1129–1136.

Chabaud-Riou M, Firestein GS. 2004. Expression and activation of mitogen-activated protein kinase kinases-3 and −6 in rheumatoid arthritis. *Am J Pathol*. 164:177–184.

Chang L, Karin M. 2001. Mammalian MAP kinase signalling cascades. Nature. 410:37–40.

Chi SC, Lo CF, Kou GH, et al. 2010. Mass mortalities associated with viral nervous necrosis (VNN) disease in two species of hatchery-reared grouper, *Epinephelus fuscogutatus* and *Epinephelus akaara* (Temminck & Schlegel). J Fish Dis. 20:185–193.

Chu JJH, Ng ML. 2003. The mechanism of cell death during West Nile virus infection is dependent on initial infectious dose. J Gen Virol. 84:3305–3314.

Cilliers T, Willey S, Sullivan WM, et al. 2005. Use of alternate coreceptors on primary cells by two HIV-1 isolates. Virology. 339:136–144.

Dashti SR, Efimova T, Eckert RL. 2001. MEK6 regulates human involucrin gene expression via a p38alpha- and p38delta-dependent mechanism. J Biol Chem. 276:27214–27220.

Doan QK, Vandeputte M, Chatain B, et al. 2017. Viral encephalopathy and retinopathy in aquaculture: A review. J Fish Dis. 40:717–742.

Dong C, Davis RJ, Flavell RA. 2002. MAP kinases in the immune response. Annu Rev Immunol. 20:55–72.

Duan X, Liang K, Yang M, et al. 2024. Genome-wide association study identifies candidate SNPs and genes associated with red-spotted grouper nervous necrosis virus infection of the giant grouper (*Epinephelus lanceolatus*). Aquaculture. 578.

Enslen H, Raingeaud J, Davis RJ. 1998. Selective activation of p38 Mitogen-activated Protein (MAP) kinase isoforms by the MAP kinase Kinases MKK3 and MKK6. J Biol Chem. 273:1741–1748.

Gan L, Seki A, Shen K, et al. 2019. The lysosomal GPCR-like protein GPR137B regulates Rag and m*TOR*C1 localization and activity. *Nat Cell Biol*. 21:614–626.

Goshima Y, Masukawa D, Kasahara Y, et al. 2019. L-dopa and its receptor GPR143 Implications for pathogenesis and therapy in Parkinson's disease. Front Pharmacol. 10:1119.

693 Hammaker D, Topolewski K, Edgar M, et al. 2012. Decreased collagen-induced
694 arthritis severity and adaptive immunity in MKK-6-deficient mice. Arthritis
695 Rheum. 64:678–687.
696 Hsu CH, Chan D, Greggio E, et al. 2010. MKK6 binds and regulates expression of
697 Parkinson's disease-related protein LRRK2. J Neurochem. 112:1593–1604.
698 Huang X, Huang Y, OuYang Z, et al. 2011. Roles of stress-activated protein kinases in
699 the replication of Singapore grouper iridovirus and regulation of the
700 inflammatory responses in grouper cells. J Gen Virol. 92:1292–1301.
701 Huang X, Huang Y, Sun J, et al.. 2009. Characterization of two grouper *Epinephelus*
702 *akaara* cell lines: Application to studies of Singapore grouper iridovirus (SGIV)
703 propagation and virus-host interaction. Aquaculture. 292:172–179.
704 Innamorati G, Piccirillo R, Bagnato P, et al. 2006. The melanosomal/lysosomal protein
705 OA1 has properties of a G protein-coupled receptor. Pigment Cell Res. 19:125–
706 135.
707 Jakobsen MR, Ellett A, Churchill MJ, et al. 2010. Viral tropism, fitness and
708 pathogenicity of HIV-1 subtype C. Future Virol. 5:219–231.
709 Jin Y, Fan Y, Yan EZ, et al. 2006. Effects of sodium ferulate on amyloid-beta-induced
710 MKK3/MKK6-p38 MAPK-Hsp27 signal pathway and apoptosis in rat
711 hippocampus. Acta Pharmacol Sin. 27:1309–1316.
712 Kim MY, Choi TY, Kim JH, et al. 2010. MKK6 increases the melanocyte dendricity
713 through the regulation of Rho family GTPases. J Dermatol Sci. 60:114–119.
714 Koyuncu OO, Hogue IB, Enquist LW. 2013. Virus infections in the nervous system.
715 Cell Host Microbe. 13:379–393.
716 Krylova RI, Dzhikidze EK. 2005. Encephalomyocarditis in monkeys. Bull Exp Biol
717 Med. 139:355–359.
718 Kyei GB, Dinkins C, Davis AS, et al. 2009. Autophagy pathway intersects with HIV-1
719 biosynthesis and regulates viral yields in macrophages. J Cell Biol. 186:255–
720 268.
721 Lai Y, Wu Y, Liu R, et al. 2020. Four-color fluorescence in-situ hybridization is useful
722 to assist to distinguish early stage acral and cutaneous melanomas from
723 dysplastic junctional or compound nevus. Diagn Pathol. 15:51.
724 Lauter G, Söll I, Hauptmann G. 2011. Multicolor fluorescent in situ hybridization to
725 define abutting and overlapping gene expression in the embryonic zebrafish
726 brain. Neural Dev. 6:10.
727 Li H, Wang S, Qian Z, et al. 2016. MKK6 from pacific white shrimp *Litopenaeus*
728 *vannamei* is responsive to bacterial and WSSV infection. Mol Immunol. 70:72–
729 83.
730 Li Y, Zhang L, Li K, et al. 2015. ZNF32 inhibits autophagy through the m*TOR* pathway
731 and protects MCF-7 cells from stimulus-induced cell death. Sci Rep. 5:9288.
732 Livak KJ, Schmittgen TD. 2001. Analysis of relative gene expression data using real-
733 time quantitative PCR and the 2(-Delta Delta C(T)) method. Methods. 25,
734 402–408.

Madeo F, Zimmermann A, Maiuri MC, et al. 2015. Essential role for autophagy in life span extension. J Clin Invest. 125:85–93.
Maiuri MC, Zalckvar E, Kimchi A, et al. 2007. Self-eating and self-killing: Crosstalk between autophagy and apoptosis. Nat Rev Mol Cell Biol. 8:741–752.
Maltese WA, Overmeyer JH. 2014. Methuosis: Nonapoptotic cell death associated with vacuolization of macropinosome and endosome compartments. *Am J Pathol.* 184:1630–1642.
Masukawa D, Nakamura F, Koga M, et al. 2014. Localization of ocular albinism-1 gene product GPR143 *in* the rat central nervous system. Neurosci Res. 88:49–57.
Mizushima N. 2007. Autophagy: Process and function. Genes Dev. 21:2861–2873.
Monel B, Compton AA, Bruel T, et al. 2017. Zika virus induces massive cytoplasmic vacuolization and paraptosis-like death in infected cells. EMBO J. 36:1653–1668.
Nishizawa T, Furuhashi M, Nagai T, et al. 1997. Genomic classification of fish nodaviruses by molecular phylogenetic analysis of the coat protein gene. Appl Environ Microbiol. 63:1633–1636.
Orvedahl A, Alexander D, Tallóczy Z, et al. 2007. HSV-1 ICP34.5 confers neurovirulence by targeting the Beclin 1 autophagy protein. Cell Host Microbe, 1:23–35.
Pierce KL, Premont RT, Lefkowitz RJ. 2002. Seven-transmembrane receptors. Nat Rev Mol Cell Biol. 3:639–650.
Qin, MM. 2019. Genetic Analysis of Transcription Factors Involved in Zebrafish Sex Differentiation. University of Macau ProQuest Dissertations & Theses, 29255447.
Qu F, Tang J, Liao J, et al. 2019. Mitogen-activated protein kinase kinase 6 is involved in the immune response to bacterial di-/tripeptide challenge in grass carp *Ctenopharyngodon idella*. *Fish Shellfish Immunol*. 84:795–801.
Raingeaud J, Gupta S, Rogers JS, et al. 1995. Pro-inflammatory cytokines and environmental stress cause p38 mitogen-activated protein kinase activation by dual phosphorylation on tyrosine and threonine. J Biol Chem. 270:7420–7426.
Raingeaud J, Whitmarsh AJ, Barrett T, et al. 1996. MKK3- and MKK6-regulated gene expression is mediated by the p38 mitogen-activated protein kinase signal transduction pathway. Mol Cell Biol. 16:1247–1255.
Ransangan J, Manin BO. 2010. Mass mortality of hatchery-produced larvae of Asian seabass, *Lates calcarifer* (Bloch), associated with viral nervous necrosis in Sabah, Malaysia. Vet Microbiol. 145:153–157.
Romero-Becerra R, Mora A, Manieri E, et al. 2022. MKK6 deficiency promotes cardiac dysfunction through MKK3-p38γ/δ-m*TOR* hyperactivation. eLife. 11: e75250.
Samaraweera P, Shen B, Newton JM, et al. 2001. The mouse ocular albinism 1 gene product is an endolysosomal protein. Exp Eye Res 72: 319-329.
Schiaffino MV, d'Addio M, Alloni A, et al. 1999. Ocular albinism: Evidence for a defect in an intracellular signal transduction system. Nat Genet. 23:108–112.

Sharma S, Ghufran SM, Ghose S, et al. 2021. Cytoplasmic vacuolation with endoplasmic reticulum stress directs sorafenib induced non-apoptotic cell death in hepatic stellate cells. Sci Rep. 11:3089.

Shi H, Ruan L, Yan X, et al. 2014. The role of *litopenaeus vannamei* p38 in white spot syndrome virus infection. Dev Comp Immunol. 44:180–185.

Shin HR, Citron YR, Wang L, et al. 2022. Lysosomal GPCR-like protein LYCHOS signals cholesterol sufficiency to m*TOR*C1. Science. 377:1290–1298.

Shubin AV, Demidyuk IV, Komissarov AA, et al. 2016. Cytoplasmic vacuolization in cell death and survival. Oncotarget. 7:55863–55889.

Souto S, Olveira JG, García-Rosado E, et al. 2019. Amino acid changes in the capsid protein of a reassortant *Betanodavirus* strain: Effect on viral replication in vitro and in vivo. J Fish Dis. 42:221–227.

Sun HY, Huang MZ, Li YW, et al. 2017. Two novel p38 MAPKs identified from Epinephelus coioides and their expression pattern in response to *Cryptocaryon irritans* infection. *Fish Shellfish Immunol*. 67:459–466.

Ueo A, Kubota M, Shirogane Y, Ohno S, et al. 2020. Lysosome-associated membrane proteins support the furin-mediated processing of the mumps virus fusion protein. J Virol. 94: e00050-20.

Wang B, Wu L, Li D, et al. 2019. Induction of pluripotent stem cells from mouse embryonic fibroblasts by Jdp2-Jhdm1b-Mkk6-Glis1-Nanog-Essrb-Sall4. Cell Rep. 27:3473–3485.

Wang G, Chen L, Qin S, et al. 2022. Cystine induced-m*TOR*C2 activation through promoting Sin1 phosphorylation to suppress cancer cell ferroptosis. Mol Nutr Food Res. 66: e2200186.

Wang G, Jiang L, Wang J, et al. 2020a. The G Protein-Coupled Receptor FFAR2 Promotes Internalization during Influenza A Virus Entry. J Virol. 94: e01707-19.

Wang Q, Liu Y, Han C, et al. 2021a. Efficient RNA virus targeting via CRISPR/CasRx in fish. J Virol. 95: e0046121.

Wang Q, Liu Y, Zhang M, et al. 2024. Slc43a2+ T cell metastasis from spleen to brain in RGNNV infected teleost. Sci China Life Sci. 67:733–744.

Wang Q, Peng C, Yang M, et al. 2021b. Single-cell RNA-seq landscape midbrain cell responses to red spotted grouper nervous necrosis virus infection. PLoS Pathog. 17: e1009665.

Wang R, Li BW, Shao NY, et al. 2021c. A novel antitumor peptide inhibits proliferation and migration and promotes apoptosis in glioma cells by regulating the MKK6/p38 signaling pathway. Neoplasma. 68:732–741.

Wang X, Zheng T, Lin L, et al. 2020b. Influenza A virus induces autophagy by its hemagglutinin binding to cell surface heat shock protein 90AA1. Front Microbiol. 11:566348.

Xu HD, Feng J, Guo ZX, et al. 2010. Detection of red-spotted grouper nervous necrosis virus by loop-mediated isothermal amplification. J Virol Methods. 163:123–128.

819 Yan H, Zhang S, Li CZ, et al. 2013. Molecular characterization and function of a p38
820 MAPK gene from *litopenaeus vannamei*. *Fish Shellfish Immunol*. 34:1421–
821 1431.
822 Yan W, Wang X, Wang W, et al. 2024. The p38/MAPK pathway as a therapeutic target
823 to prevent therapeutic escape of breast cancer stem cells. Sci China Life Sci.
824 67:1867–1880.
825 Yang B, Xue Q, Guo J, et al. 2020. Autophagy induction by the pathogen receptor
826 NECTIN4 and sustained autophagy contribute to peste des petits ruminants
827 virus infectivity. Autophagy. 16:842–861.
828 Yong CY, Yeap SK, Omar AR, et al. 2017. Advances in the study of nodavirus. PeerJ.
829 5: e3841.
830 Yoshizawa T, Hammaker D, Boyle DL, et al. 2009. Role of MAPK kinase 6 in arthritis:
831 Distinct mechanism of action in inflammation and cytokine expression. J
832 Immunol. 183:1360–1367.
833 Yu L, Chen Y, Tooze SA. 2018. Autophagy pathway: Cellular and molecular
834 mechanisms. Autophagy. 14:207–215.
835 Zhang W, Yang X, Li Y, et al. 2022a. GCAF(TMEM251) regulates lysosome biogenesis
836 by activating the mannose-6-phosphate pathway. Nat Commun. 13:5351.
837 Zhang WW, Jia P, Lu XB, et al. 2022b. Capsid protein from red-spotted grouper nervous
838 necrosis virus induces incomplete autophagy by inactivating the HSP90ab1-
839 AKT-M*TOR* pathway. Zool Res. 43:98–110.
840

841 **Figure**

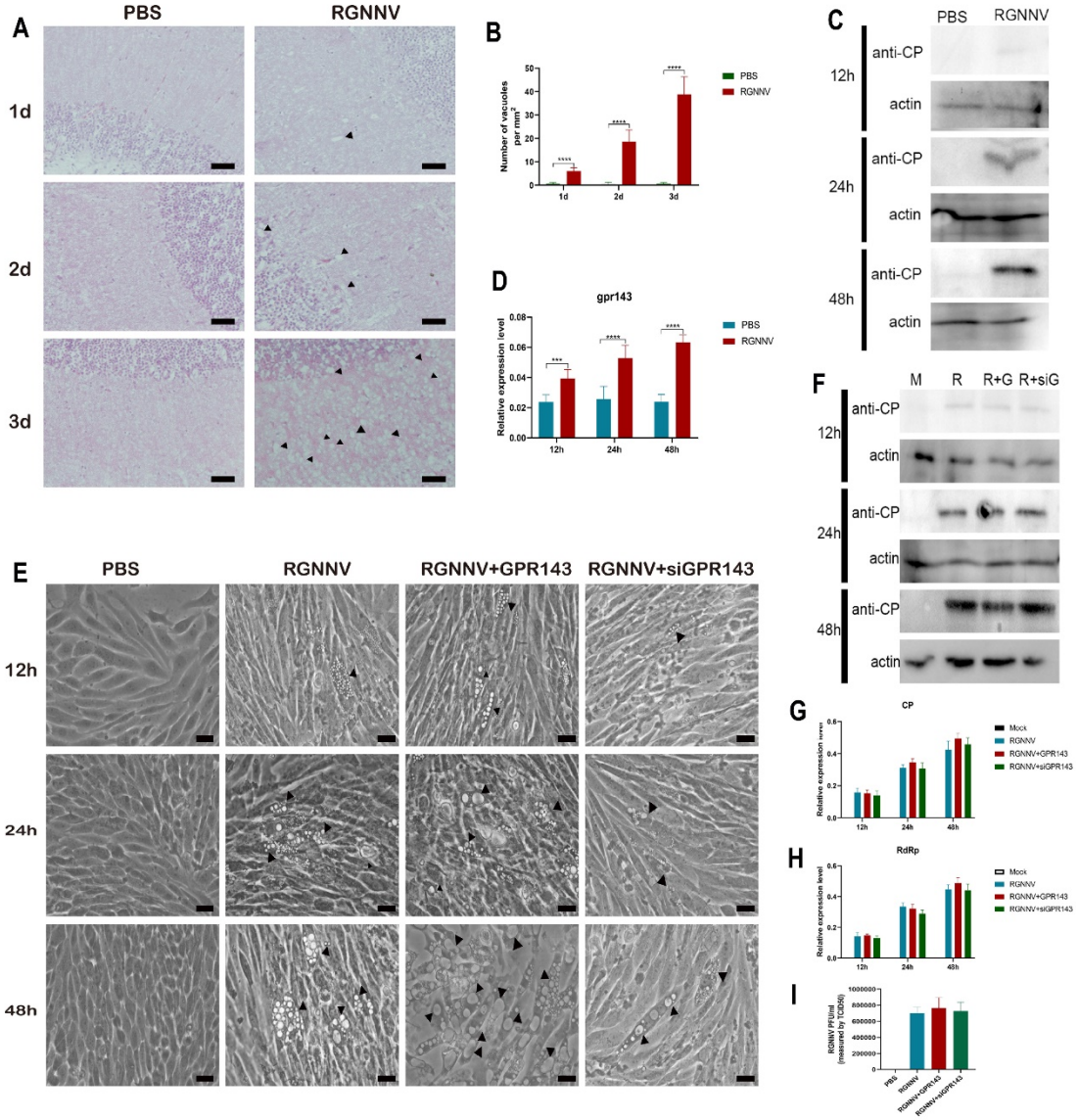


842

843 Figure 1. GPR143 promotes RGNNV-induced cell vacuolation. (**A**) Brain histology of
844 PBS- and RGNNV-treated fish, with vacuoles indicated using black arrowheads. 1 d, 3
845 d and 5 d indicate 1 day, 3 days, and 5 days after RGNNV infection. Scale bar: 50
846 μmol/L. (**B**) Statistical analysis of the number of vacuoles per mm2. Five fish were
847 analyzed, with three images taken for each fish. ****$P$<0.000 1. (**C**) Levels of *cp* in
848 grouper brains were determined via western blotting at 1 day, 3 days, and 5 days
849 following RGNNV infection. M: Mock, R: RGNNV, R+G: RGNNV+GPR143 R+siG:
850 RGNNV+siGPR143 (**D**) *gpr143* expression in brain tissue from PBS- and RGNNV-
851 treated groupers ($n$=10). ***$P$<0.001, ****$P$<0.000 1. (**E**) Cell morphology and

cytopathic effects (vacuolation) in GS cells without treatment (Mock) or treated with RGNNV or RGNNV+GPR143 or RGNNV+siGPR143 at 12h, 24h, and 48h. Scale bar=25 μmol/L. (**F**) Levels of CP in GS cells without treatment (Mock) or treated with RGNNV or RGNNV+GPR143 or RGNNV+siGPR143 at 12h, 24h, and 48 h. (**G**) Expression of *cp* in GS cells without treatment (Mock) or treated with RGNNV or RGNNV+GPR143 or RGNNV+siGPR143 at 12h, 24h, and 48h (*n*=4). (**H**) Expression of *rdrp* in GS cells without treatment (Mock) or treated with RGNNV or RGNNV+GPR143 or RGNNV+siGPR143 at 12h, 24h, and 48h (*n*=4). (**I**) RGNNV PFU per milliliter measured as $TCID_{50}$ with siGPR143 treated.

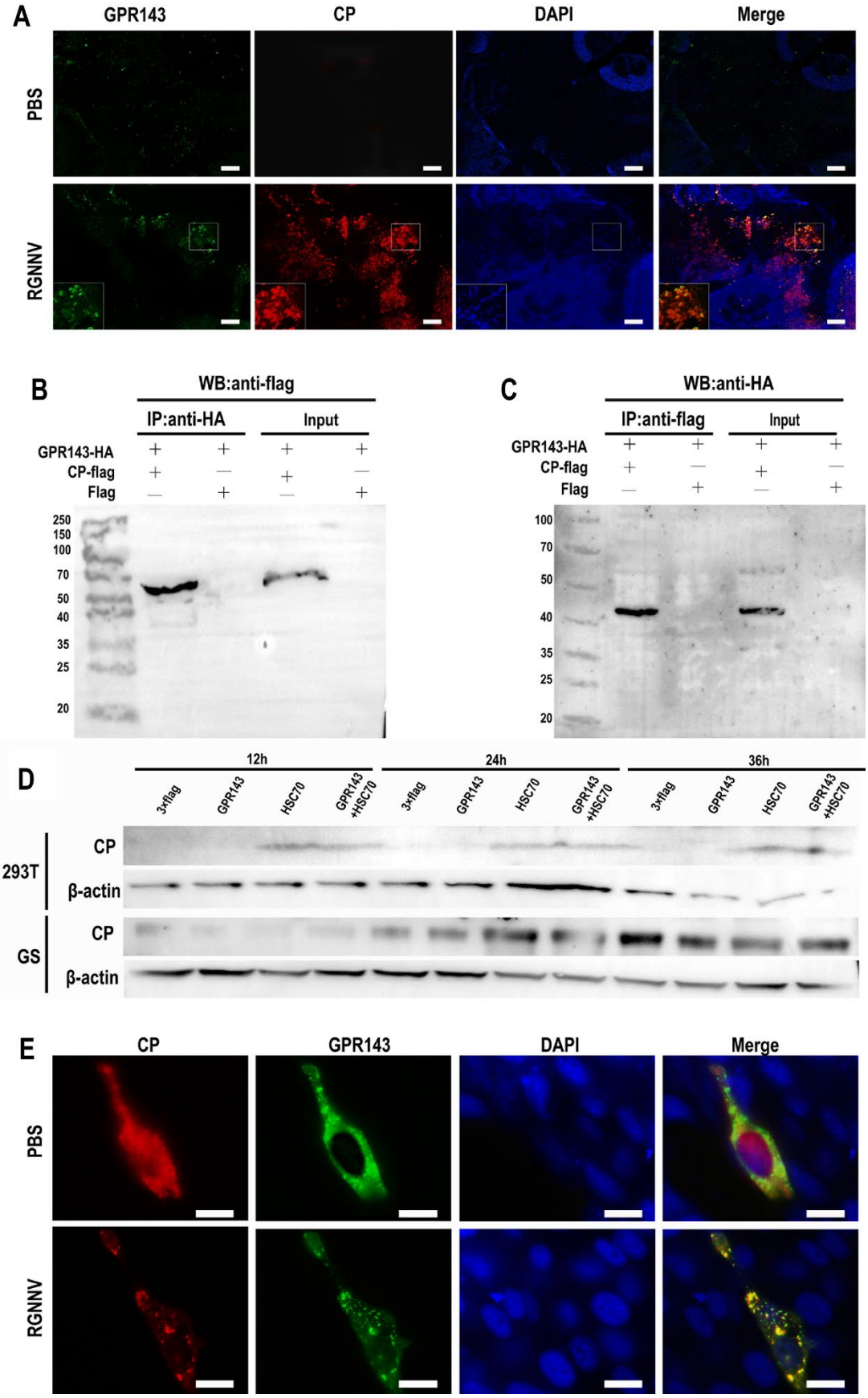

Figure 2. GPR143 binds to the RGNNV CP but is not a receptor. (**A**) Multicolor FISH staining to validate the GPR143 and CP states. FISH staining showed that *gpr143* and *cp* were co-located in the grouper brain; moreover, the binding of GPR143 to CP in the brains of the RGNNV infection fish was observed. The white box area shows a magnified view of the lower left corner. Scale bar: 200 μmol/L. (**B**) Interaction between GPR143 and CP. Co-IP was performed on the plasmid-co-transfected GS cells. Cells were treated with an anti-HA antibody, and western blotting was performed using an anti-FLAG antibody. HA-tagged GPR143 co-precipitated with FLAG-tagged CP, whereas control FLAG did not coprecipitate. The expected size of CPs was 54.28 kD. (**C**) Interaction between GPR143 and CP. Co-IP was performed on plasmid-co-transfected GS cells using an anti-FLAG antibody, and western blotting was performed using an anti-HA antibody. HA-tagged GPR143 co-precipitated with FLAG-tagged CP, whereas control FLAG did not coprecipitate. The expected size of GPR143 protein was 44.59 kD. (**D**) After overexpression of GPR143 HSC70, and GPR143+HSC70 in HEK293T and GS cells, RGNNV was infected, and CP expression in the cells was detected. (**E**) Co-transfection with *GFP-GPR143* and *Cherry-CP* after PBS or RGNNV treatment. Upon PBS treatment, GPR143 and CP did not cluster. After RGNNV infection, GPR143 and CP clustered together. Scale bar=10 μmol/L.

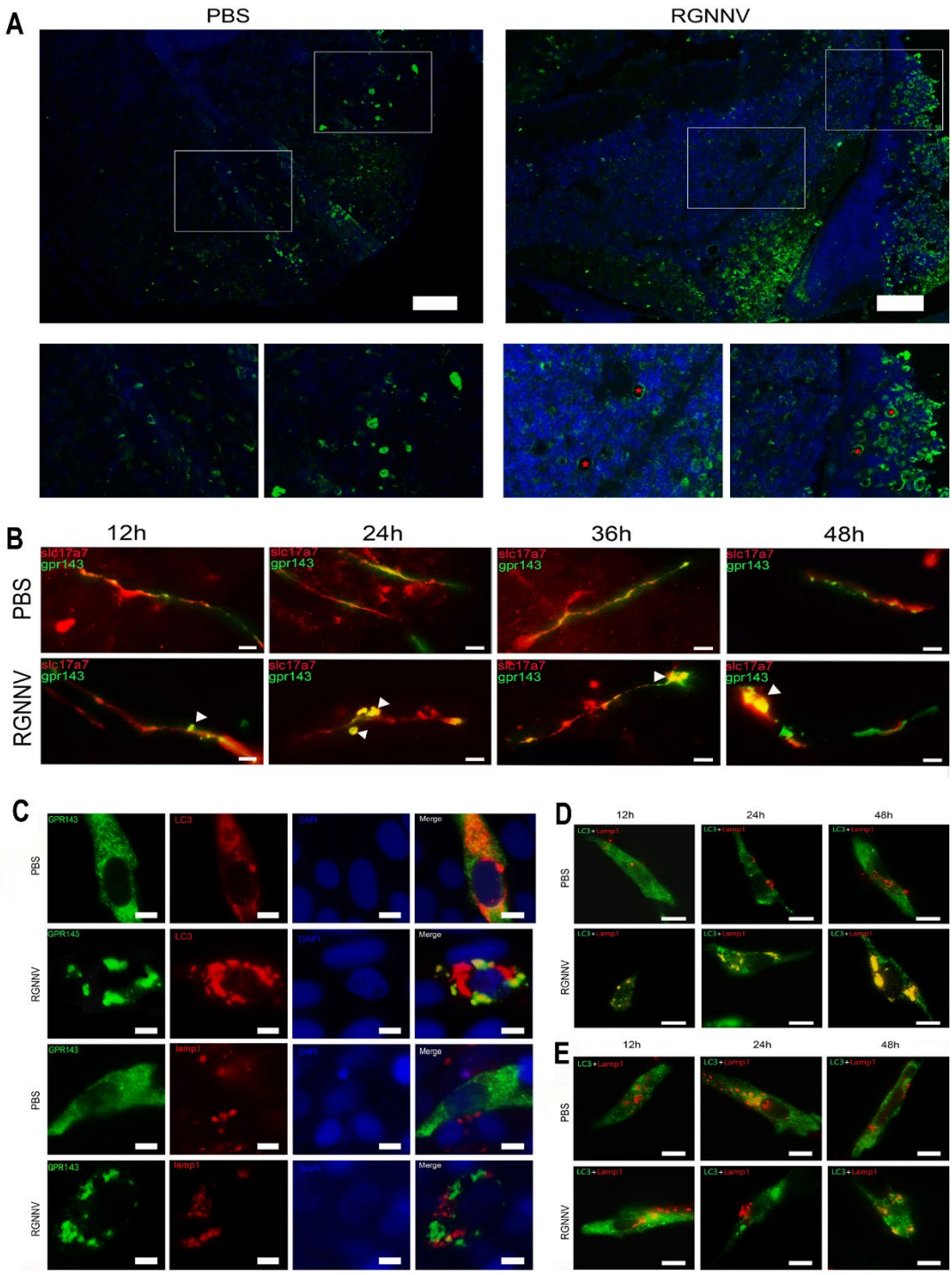


Figure 3. GPR143 plays a vital role in the binding of autophagosomes and lysosomes. (**A**) Status of GPR143 in infected and uninfected grouper brain tissue. GPR143 -positive signals were few and dispersed in uninfected brain tissue, whereas GPR143 localized around vacuoles in RGNNV-infected brain tissue. The red five-pointed stars represent the vacuoles. The bottom row shows a magnified view of the boxed areas in the top row (panorama). Scale bar=100 μmol/L. (**B**) Multicolor FISH staining to

validate the GPR143 and virus target cell states after virus infection 12h, 24h, 36h and 48h. FISH staining showed that gpr143 and virus target cell marker gene slc17a7 were co-located in the RGNNV infection cell; moreover, RGNNV infection will induce the formation of aggregated gpr143 in the target cells and forming vacuoles. The white triangle indicates that gpr143 and slc17a7 aggregate. Scale bar: 20 μmol/L. (**C**) Co-transfection with GFP-GPR143 and Cherry-LC3 or Cherry-LAMP1 after PBS treatment or RGNNV infection. Following PBS treatment, GPR143 and LC3 or LAMP1 did not cluster together. After RGNNV infection, GPR143 and CP clustered together, but only a small amount of GPR143and LAMP1 clustered together. Scale bar=10 μmol/L. (**D**) Co-transfection with GFP-LC3 and Cherry-LAMP1 after PBS or RGNNV infection. After PBS treatment, LC3 and LAMP1 did not cluster together. After RGNNV infection, LC3 and LAMP1 clustered together at 12, 24, and 48 h after infection. Scale bar=10 μmol/L (**E**) Co-transfection with GFP-LC3 and Cherry-LAMP1 after PBS treatment or RGNNV infection in which siRNA was used to inhibit GPR143 Upon PBS treatment, LC3 and LAMP1 did not cluster together at 12, 24, or 48h after treatment. After RGNNV infection, LC3 and LAMP1 did not cluster together at 12 or 24h, but a small amount of LC3 and LAMP1 clustered together at 48h after RGNNV infection. Scale bar=10 μmol/L.

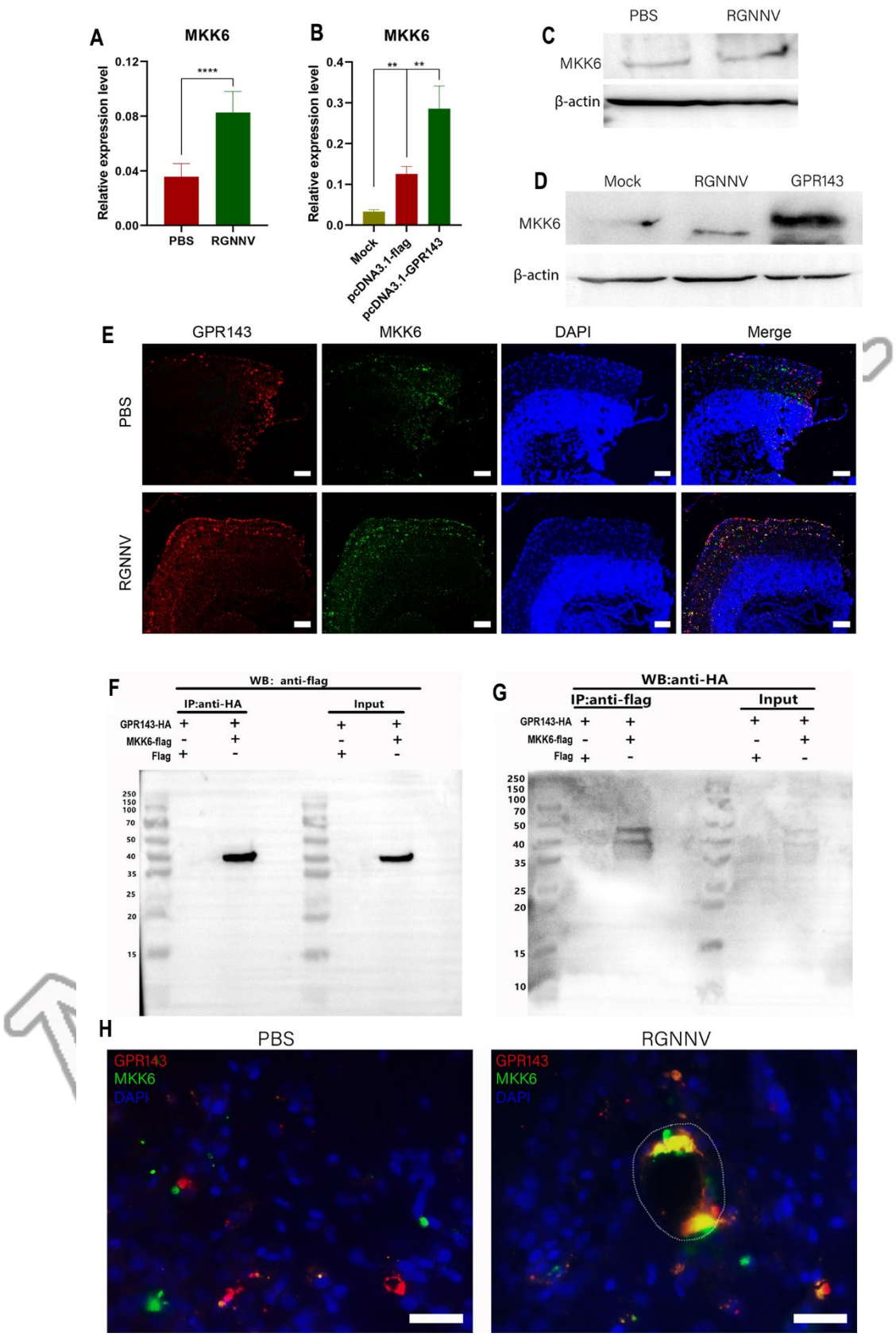


909

910 Figure 4. GPR143 regulates RGNNV-induced vacuolization through MKK6. (**A**)

911 Expression of *mkk6* in the brain tissue of PBS- or RGNNV-treated fish (*n*=8).

****$P$<0.000 1. (**B**) Expression of *mkk6* in the Mock, RGNNV+pcDNA3.1-3×flag, and RGNNV+pcDNA3.1-GPR143 groups after RGNNV infection ($n$=4). **$P$<0.01. (**C**) Western blotting of MKK6 in brain tissue from PBS-or RGNNV-treated fish. (**D**) Western blotting of MKK6 in brain tissue from the Mock, RGNNV, and RGNNV+GPR143 groups. (**E**) Multicolor FISH staining to validate the *gpr143* and *mkk6* states. FISH staining showed that *gpr143* and *cp* mRNA were not co-located in the PBS-treated grouper brain but were co-located after RGNNV infection. Scale bars=200 μmol/L. (**F**) Co-IP performed on plasmid-co-transfected GS cells using an anti-HA antibody, and western blotting was performed using an anti-FLAG antibody to monitor the interaction between GPR143 and MKK6. HA-tagged GPR143 was co-precipitated with FLAG-tagged MKK6, whereas the control FLAG could not be co-precipitated. (**G**) Co-IP was performed on plasmid-co-transfected GS cells using an anti-FLAG antibody, and western blotting was performed using an anti-HA antibody to monitor the interaction between GPR143 and MKK6. HA-tagged GPR143 was co-precipitated with FLAG-tagged MKK6, whereas the control FLAG could not be co-precipitated. (**H**) Multicolor FISH staining to validate the *gpr143* and *mkk6* mRNAs aggregation showed almost no co-localization of *gpr143* and *mkk6* in PBS-treated brains but revealed co-localization around the vacuoles during RGNNV infection. The white dotted line denotes a vacuole. Scale bar=20 μmol/L.

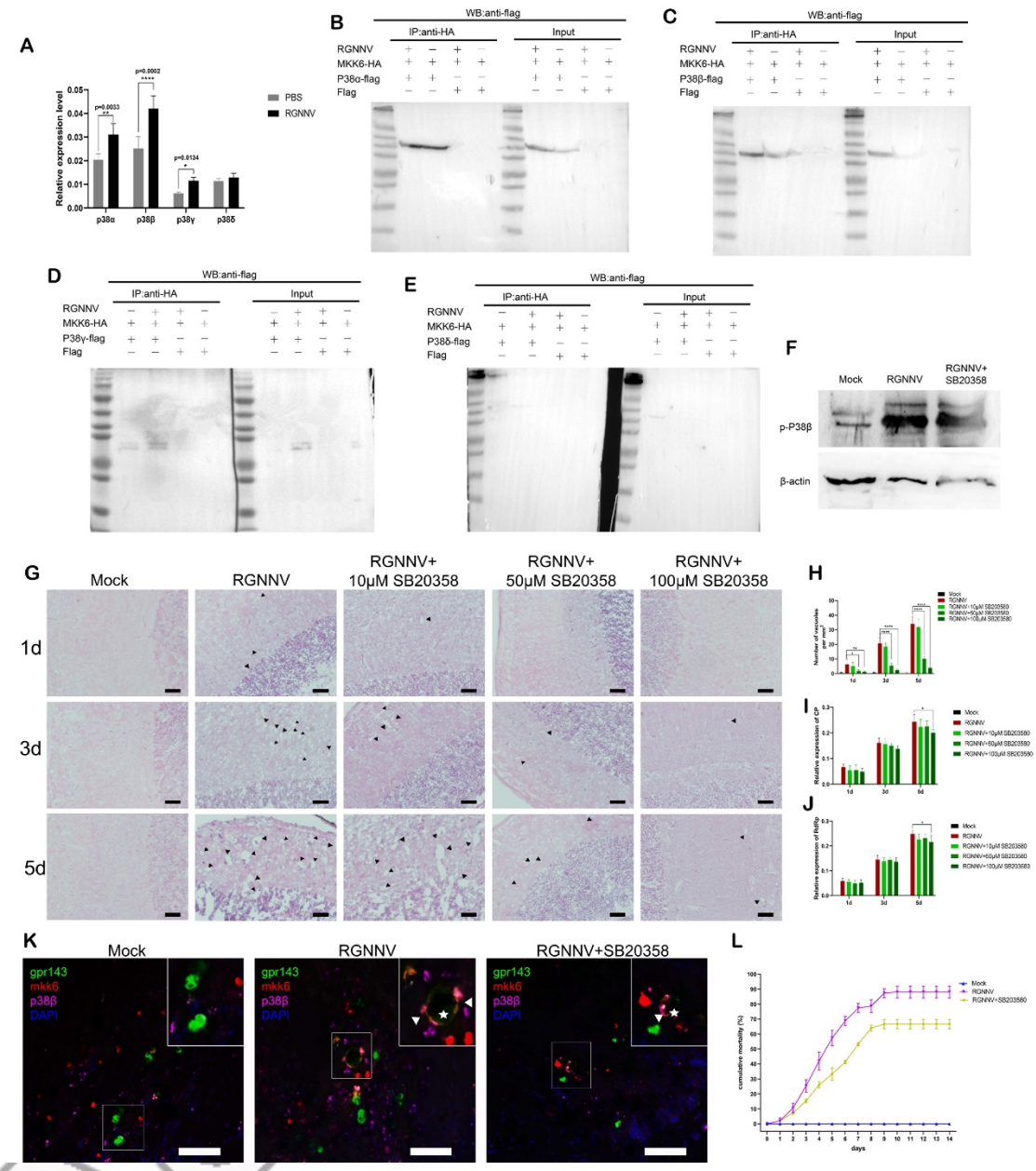


Figure 5. MKK6 regulates the vacuolization induced by RGNNV through p38. (**A**) Expression of *p38α*, *p38β*, *p38γ*, and *p38δ* in RGNNV-treated fish brain (*n*=8). (**B–E**) Binding of MKK6 and P38α, P38β, P38γ, or P38δ before and after RGNNV infection. (**F**) Phosphorylation of P38β in brain tissue from Mock-, RGNNV-, and RGNNV+SB20358- treated fish. (**G**) Brain histology of Mock, RGNNV, RGNNV+ 10μmol/LSB20358, RGNNV+50μmol/LSB20358 and RGNNV+100μmol/LSB20358-treated fish. The black arrowhead indicates vacuoles. Scale bar=50 μmol/L. (**H**) Statistical analysis of the number of vacuoles per mm$^2$. Five fish were analyzed. **P*<0.05, ***P*<0.01, *****P*<0.000 1. (**I**) Expression of cp in Mock-, RGNNV-,

RGNNV+10μmol/LSB20358, RGNNV+50μmol/LSB20358 and RGNNV+100μmol/LSB20358-treated fish brain ($n$=5). (**J**) Expression of rdrp in Mock-, RGNNV-, RGNNV+10μmol/LSB20358, RGNNV+ 50μmol/LSB20358 and RGNNV+100μmol/LSB20358-treated fish brain ($n$=5). (**K**) Multicolor FISH staining was used to validate the *gpr143*, *mkk6*, and *p38β* localization in brain tissue. Following RGNNV infection, *gpr143*, *mkk6*, and *p38β* mRNAs were found to co-localization around the vacuoles, and treatment with SB203580 reduced this co-localization. Scale bar=50 μmol/L. White arrowhead indicates the co-localization of *gpr143*, *mkk6*, and *p38β* mRNA; white five-pointed stars represent the vacuoles. (**L**) Cumulative mortality rate for each group of orange-spotted groupers during the 14-day experimental period after the different treatments (Mock, RGNNV, RGNNV + SB20358).

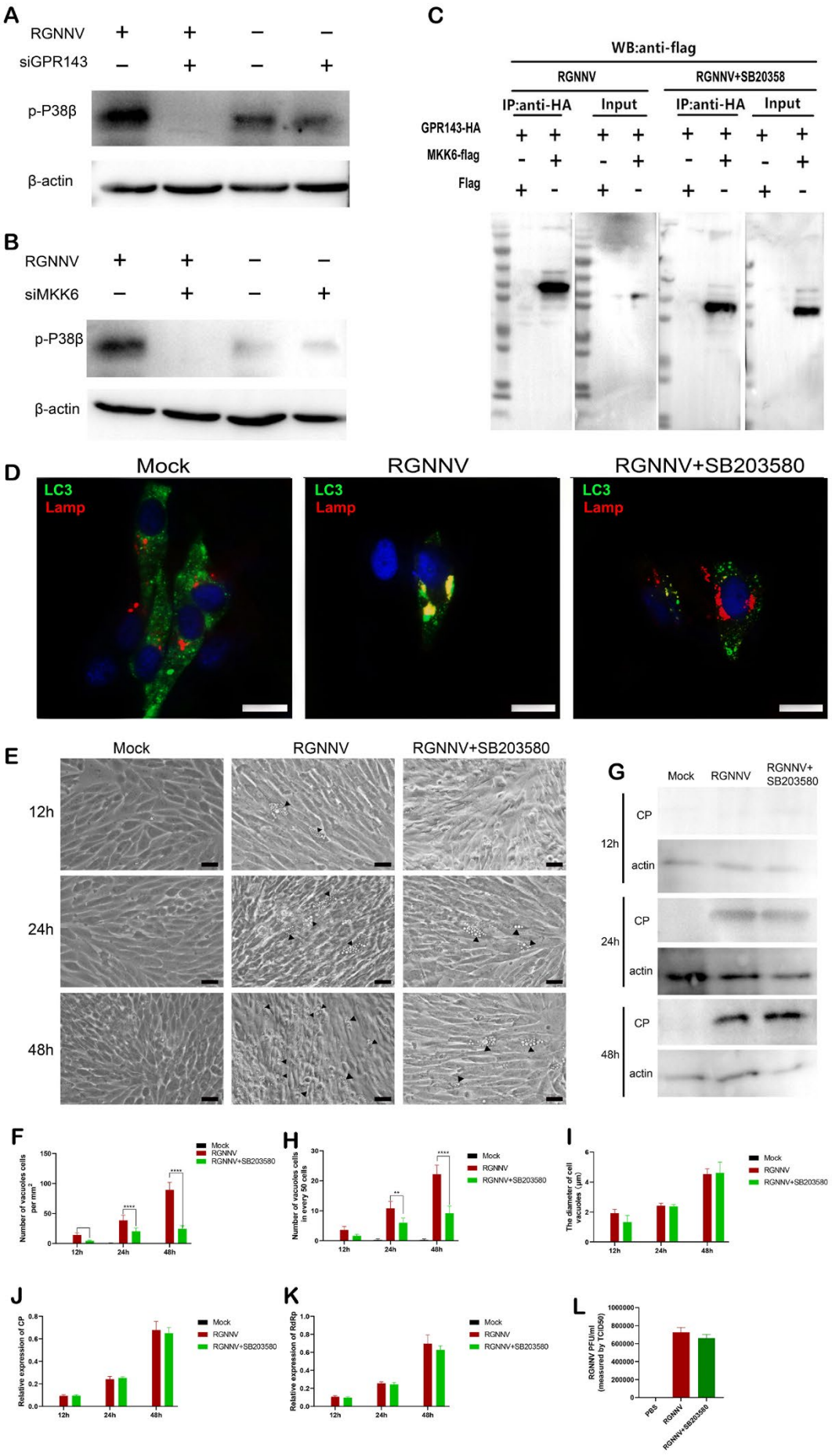




Science Press
ZR Zoological Research

Figure 6. P38 is a downstream target of MKK6 and regulates the RGNNV-induced binding of autophagosomes and lysosomes. (A) Inhibition of GPR143 expression by siRNA inhibits P38β phosphorylation induced by RGNNV. (B) Inhibition of MKK6 expression by siRNA inhibited P38β phosphorylation induced by RGNNV. (C) Inhibition of P38 function by SB203580 did not affect RGNNV-induced binding of GPR143 to MKK6. (D) Co-transfection with GFP-LC3 and Cherry-LAMP1 after Mock, RGNNV, and RGNNV+SB203580 treatments. In the Mock group, LC3 and LAMP1 did not cluster together. In the RGNNV infection group, numerous LC3 and LAMP1 clusters were combined into larger clumps. In the RGNNV+SB203580 treatment, a reduced amount of LC3 and LAMP1 clustered and did not combine into larger clumps. Scale bar=10 μmol/L. (E) Cell morphology and CPEs (vacuolation) after Mock, RGNNV, and RGNNV+SB203580 treatment groups at 12h, 24h, and 48h. The black arrowhead indicates vacuoles. Scale bar=25 μmol/L. (F) Statistical analysis of the number of vacuoles cells per mm2. Five images were analyzed in each group. ****$P$<0.000 1. (G) Levels of CP in GS cells without treatment (Mock) or treated with RGNNV or RGNNV+SB203580 at 12h, 24h, and 48h. (H) Statistical analysis of the number of vacuoles cells per every 50 cells. **$P$<0.01, ****$P$<0.000 1. (I) Statistical analysis of the diameter of cell vacuoles. (J) Expression of *cp* in the GS cells without treatment (Mock) or treated with RGNNV or RGNNV+SB203580 at 12h, 24h, and 48h ($n$=4). (K) Expression of *rdrp* in the GS cells without treatment (Mock) or treated with RGNNV or RGNNV+SB203580 at 12h, 24h, and 48h ($n$=4). (L) RGNNV PFU per milliliter measured as $TCID_{50}$ with SB203580 or without SB203580 treated.

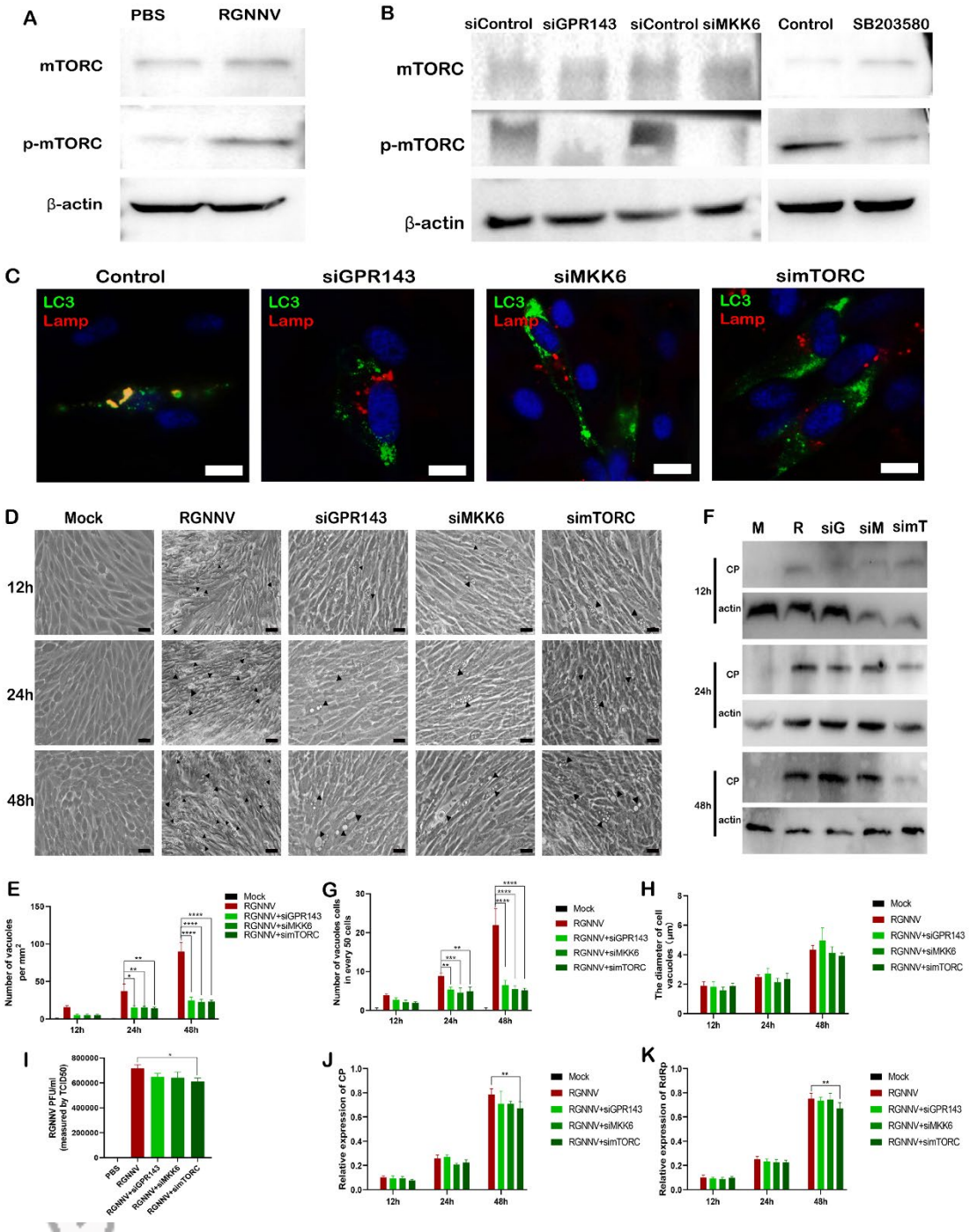


Figure 7. mTORC is a downstream regulatory element of p38, and its phosphorylation is crucial for cellular vacuolation induced by RGNNV. (A) Western blotting of mTORC and p-mTORC in PBS- or RGNNV-treated fish brain. (B) Western blotting showing the expression and phosphorylation of mTORC protein after inhibition of GPR143 MKK6, or p38 followed by treatment with RGNNV. (C) Co-transfection with *GFP-LC3* and Cherry-LAMP1 after inhibition of GPR143 MKK6, or mTORC, followed by treatment with RGNNV. In the RGNNV group, LC3 and LAMP1 clustered together and

combined into larger clumps, whereas in the siGPR143 +RGNNV, siMKK6+RGNNV, and simTORC+RGNNV treatment groups, LC3 and LAMP1 did not cluster together. Scale bar=10 μmol/L. (D) Cell morphology and CPEs (vacuolation) in Mock, RGNNV, siGPR143+RGNNV, siMKK6+RGNNV, and simTORC+RGNNV treatment groups at 12h, 24h, and 48h. Scale bar=25 μmol/L. (E) Statistical analysis of the number of vacuoles cells per mm2. Five images were analyzed in each group. *$P$<0.05, ** $P$<0.01, ****$P$<0.000 1. (F) Levels of CP in Mock, RGNNV(R), siGPR143+RGNNV (siG), siMKK6+RGNNV (siM), and simTORC+RGNNV (simT) treatment groups at 12h, 24h, and 48h. (G) Statistical analysis of the number of vacuoles cells per every 50 cells. **$P$<0.01, ****$P$<0.000 1. (H) Statistical analysis of the diameter of cell vacuoles. (I) RGNNV PFU per milliliter measured as $TCID_{50}$ with siGPR143 siMKK6 and simTORC treated. *$P$<0.05. (J) Expression of *cp* in Mock, RGNNV, siGPR143 +RGNNV, siMKK6+RGNNV, and sim*TORC*+RGNNV treatment groups at 12h, 24h and 48h ($n$=4), **$P$<0.01. (K) Expression of *rdrp* in Mock, RGNNV, siGPR143+RGNNV, siMKK6+RGNNV, and simTORC+RGNNV treatment groups at 12h, 24h, and 48h ($n$=4), **$P$<0.01.

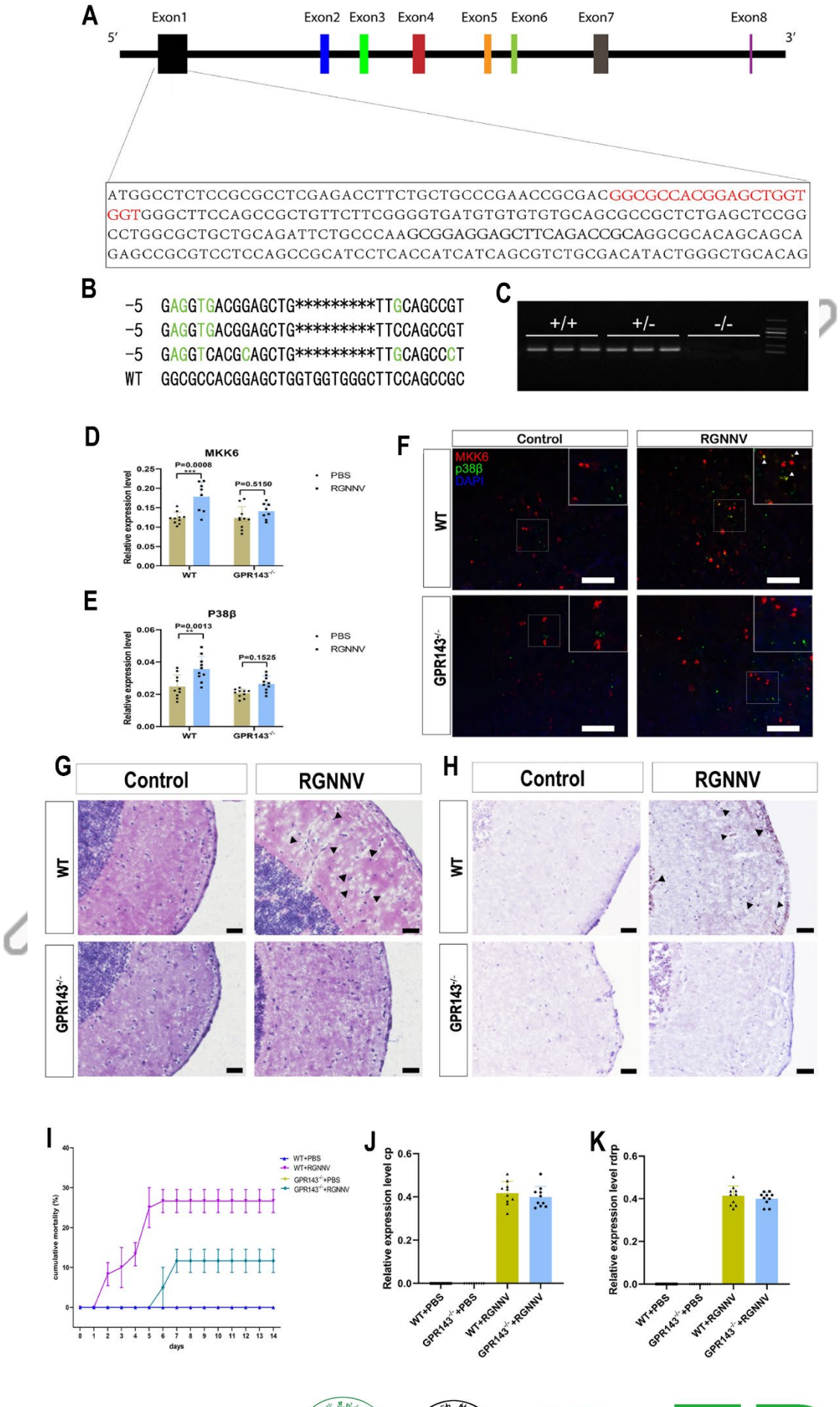




Science Press
ZR Zoological Research

Figure 8. Knockout of GPR143 zebrafish mutants shows a phenomenon similar to that of grouper and involves the GPR143 –MKK6–P38 pathway. (A) Genomic structure of the zebrafish GPR143 gene, consisting of eight exons (colored boxes) and seven introns (black lines). The partial sequence of the first exon is shown in the box below, with the CRISPR/Cas9 target site marked using a red line and highlighted in the sequence. (B) Sequence confirmation of the mutations. (C) RT-qPCR assay for *gpr143* expression in the brain using mutation-specific primers. (D) *mkk6* expression in WT and GPR143$^{-/-}$ knockout zebrafish, both uninfected and infected with RGNNV. (E) Expression of *p38β* in WT and GPR143$^{-/-}$ knockout zebrafish, infected and uninfected with RGNNV. (F) Multicolor FISH staining to validate the localization of *mkk6* and *p38β* mRNA in brain tissue of WT and GPR143 knockout zebrafish treated with PBS or RGNNV. Co-localization of *mkk6* and *p38β* was observed following RGNNV infection in WT zebrafish, but not in GPR143 mutants. Scale bar = 50 μmol/L. (G) Brain histology of WT and GPR143$^{-/-}$ zebrafish, both uninfected and infected with RGNNV, with black arrowheads indicating vacuoles. Scale bar = 50 μmol/L. (H) TUNEL assay showing brain cell apoptosis in WT and GPR143$^{-/-}$ zebrafish, both uninfected and infected with RGNNV, with black arrowheads indicating TUNEL-positive signals. Scale bar = 50 μmol/L. (I) Cumulative mortality rate for each group of WT and GPR143$^{-/-}$ zebrafish over a 14-day period after PBS treatment or RGNNV infection. (J) Expression of *cp* in WT and GPR143$^{-/-}$ zebrafish after RGNNV treatmented 24h ($n$=10). (K) Expression of *rdrp* in WT and GPR143$^{-/-}$ zebrafish after RGNNV treatmented 24h ($n$=10).

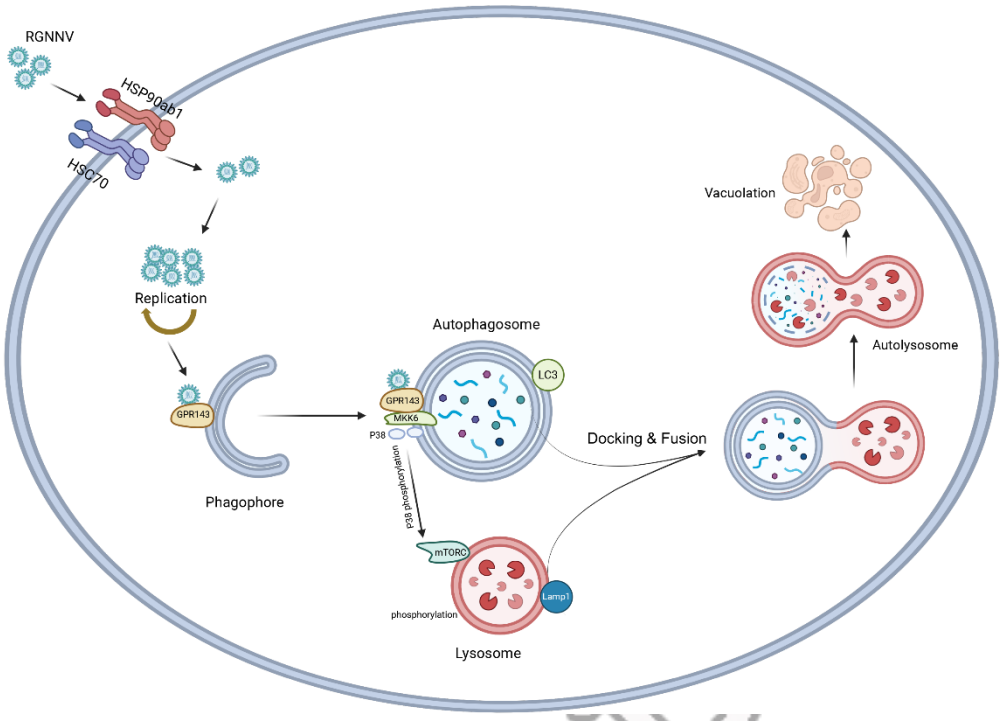


1033

1034 Figure 9. Conceptual model of RGNNV-mediated cellular vacuolation via the GPR143

1035 pathway. RGNNV first binds to HSC70 or HSP90ab1 to enter the cell, where it interacts

1036 with GPR143 on a phagophore. This interaction promotes the phosphorylation of p38

1037 via MKK6, which in turn stimulates m*TORC* phosphorylation, enhancing

1038 autophagosome and lysosome binding, culminating in cellular vacuolation.

1039

# GPR143 通过 MKK6-p38 通路调控硬骨鱼中病毒诱导的细胞空泡化

**王庆[13]，梁建韬[1]，何学泓[1]，韦丽云[1]，闫旭[1]，蒙扬辉[1]，朱秀茹[1]，青宋丽[1]，赵会宏[13]，吴锦辉[2]，秦启伟[134*].**

[1] 华南农业大学海洋学院，广东 广州 510642

[2] 广东省农业技术推广中心，广东 惠州 529699

[3] 广州南沙华农渔业研究院，广东 广州 511457

[4] 海洋生物学与生物技术实验室，海洋科学与技术国家实验室（青岛），山东 青岛 266000

[*] 通讯作者:秦启伟，邮箱：qinqw@scau.edu.cn.

**摘要**

诱导细胞空泡化是很多病毒引起细胞死亡的重要步骤，但其机制尚不明确。神经坏死病毒（NNV）感染会引起鱼类脑组织细胞显著的空泡化。G 蛋白偶联受体（GPCR）在调控自噬体功能和细胞空泡形成方面发挥重要作用。我们前期通过全基因组关联分析发现 GPR143 是石斑鱼抗赤点石斑鱼神经坏死病毒（RGNNV）的关键候选靶基因。本研究以斜带石斑鱼和 RGNNV 为模型，探究 GPR143 在神经坏死病毒诱导细胞空泡化中的作用。结果表明，GPR143 会加速自噬体与溶酶体结合促进 RGNNV 诱导细胞的空泡化。进一步发现，RGNNV 感染诱导 GPR143 与 MKK6 结合，而 MKK6 又通过调控 p38 磷酸化来影响雷帕霉素靶蛋白（m*TOR*）通路，进而促进自噬体与溶酶体结合诱发细胞质空泡化。最后通过 GPR143 基因敲除斑马鱼模型证实，缺失 GPR143 可显著减轻脑部空泡化并降低鱼苗死亡率。这些结果表明 GPR143 通过 MKK6-p38 通路介导硬骨鱼类病毒诱导的细胞空泡化。本研究揭示了病毒在脊椎动物中引发空泡化的新途径。

**关键词:** 空泡化; GPR143　MKK6-p38; RGNNV; 硬骨鱼